Water Air Soil Pollut (2025) 236:872
https://doi.org/10.1007/s11270-025-08526-6

Effective Adsorption of Pharmaceuticals by Plant Based-Activated Biochar

Zahra Shirani · Victor Carrasco-Navarro · Jouni Sorvari

Received: 15 May 2025 / Accepted: 20 August 2025 / Published online: 3 October 2025

Abstract Pharmaceuticals play a crucial role in human health and animal well-being. However, wastewater treatment plants often have limited removal efficiency for these substances, classifying pharmaceuticals as persistent environmental contaminants. This study investigates activated biochar produced from *Anthriscus sylvestris* (ASBS) for the adsorption of tetracycline (TET) and ciprofloxacin (CIPF) using batch and fixed-bed column experiments. The adsorbent showed high adsorption capacities (402.75 mg g^{-1} for TET; 582.18 mg g^{-1} for CIPF) and equilibrium was achieved after 1400 and 380 min, respectively. Adsorption followed the Langmuir and the pseudo-second-order models and was governed by multiple interactions, such as π-π electron donor–acceptor (EDA) interactions, cation-π bond, and hydrogen bonding. Furthermore, fixed-bed column studies confirmed the potential for continuous treatment under various concentrations and flow rates. Overall, this study demonstrates a practical method for producing a low-cost adsorbent that can effectively reduce pharmaceutical contamination in aqueous solutions.

Highlights

- Anthriscus sylvestris-derived activated biochar (ASBS) removed pharmaceuticals.
- ASBS showed high sorption for tetracycline (TET) and ciprofloxacin (CIPF).
- 0.25 g L^{-1} of ASBS removed ca. 99.9% and 99.8% of TET and CIPF, respectively.
- TET and CIPF sorption on ASBS was endothermic.
- The adsorption mechanism was explained by π–π EDA interaction and H-bonding.

Keywords Biochar modification · Water treatment · Ciprofloxacin · Tetracycline · Adsorption mechanisms · Fixed-bed-column studies

1 Introduction

Antibiotics such as tetracycline (TET) and ciprofloxacin (CIPF) are widely used to treat and prevent infectious diseases (Fiori et al., 2022; Mangla et al., 2022).

Supplementary Information The online version contains supplementary material available at https://doi.org/10.1007/s11270-025-08526-6.

Z. Shirani (✉) · V. Carrasco-Navarro · J. Sorvari
Department of Environmental and Biological Sciences, University of Eastern Finland, P.O. Box 1627, FI-70211 Kuopio, Finland
e-mail: zahra.shirani@uef.fi

Present Address:
J. Sorvari
Natural Resources Institute Finland (Luke), Latokartanonkaari 9, FI-00790 Helsinki, Finland

These antibiotics are frequently detected in surface, drinking, and wastewater worldwide at concentrations ranging from ng L^{-1} to µg L^{-1} and have been shown to persist even after conventional wastewater treatment (Singh et al., 2024). By targeting essential cellular processes, such as protein synthesis and DNA replication, these bactericidal antibiotics impair bacterial survival and inhibit the spread and development of infections in the human body (Martins et al., 2015; Yu et al., 2016).

Discharged antibiotics further accumulate in water bodies globally (Ali et al., 2018; Mangla et al., 2022), causing severe negative impacts on human and environmental health, such as chronic allergic reactions (Mao et al., 2016; Sun et al., 2018) and the formation of bacterial populations that are resistant to antibiotics (Sun et al., 2018; Zeng et al., 2018). TET has potent antibacterial properties (Liao et al., 2013; Fiori et al., 2022), and is the second most widely used and produced antibiotic worldwide (Guler & Sarioglu, 2014; Fiori et al., 2022). CIPF, a second-generation quinolone antibiotic (Yu et al., 2016; Sun et al., 2018), is highly resistant to biodegradation (Yu et al., 2016; Sun et al., 2018). Such persistence demands innovative and effective removal strategies that are both practical and sustainable.

An effective approach to minimize these pharmaceuticals in natural waters is to remove them in wastewater treatment plants (WWTPs) before discharge. However, conventional treatments in WWTPs often fail to completely remove pharmaceuticals (including TET and CIPF) (Ali et al., 2018; Fiori et al., 2022; Mangla et al., 2022), with removal efficiencies below 50% for most compounds (Vieno et al., 2017). Various technologies have been adopted for treating wastewater containing antibiotics, including photocatalytic degradation (He et al., 2016; Gholami et al., 2020), electro-degradation (Brinzila et al., 2012; Fiori et al., 2022), and oxidation (He et al., 2016; Dhiman & Sharma, 2018;). However, their application is often limited due to high cost, energy consumption, or formation of toxic by-products (Martins et al., 2015; Zeng et al., 2019). Therefore, adsorption remains one of the most promising physicochemical technologies due to its simplicity, cost-effectiveness, and scalability potential (Mangla et al., 2022).

Various adsorbents have been studied, including activated carbon (Sayğılı & Güzel, 2016), graphene oxide (Ma et al., 2015), and carbon nanotubes (Yu et al., 2016). However, all these adsorbents can be costly to produce at scale (Wang et al., 2018; Mangla et al., 2022). Consequently, there is a need for cheaper, renewable alternatives with comparable performance. Biochar offers a more sustainable and low-cost alternative, especially when derived from abundant or invasive biomass sources (Wang et al., 2018; Mangla et al., 2022). Biochar is defined as a porous carbon material derived through the pyrolysis of biomass under limited oxygen conditions (Shirani et al., 2024). Its adsorption capability depends on parameters such as the biomass origin, surface area, porosity, and surface functional groups, all of which can be improved through chemical or physical activation (Wang et al., 2018; Mangla et al., 2022). For instance, alkali activation with NaOH, can improve porosity and introduce oxygen-containing functional groups that facilitate multiple adsorption pathways (Wang et al., 2018).

Anthriscus sylvestris, commonly known as cow parsley, is a short-lived, perennial tall herb from the Apiaceae family (Magnússon, 2011; Miller & D'auria, 2011). It is indigenous to parts of Asia and Europe, including Finland (Magnússon, 2011; Miller & D'auria, 2011). *A. sylvestris* has applications in traditional medicine for the treatment and prevention of several diseases, including eczema, hemorrhoids, and liver problems (Vyas et al., 2012). Nowadays, this herb is considered an invasive species in many countries, such as The Netherlands, Canada and Iceland (Miller & D'auria, 2011; Halldórsson, 2012; Seegers et al., 2018). Using this underutilized invasive species not only provides a sustainable feedstock but also supports local ecosystem management efforts.

This study explores the use of chemically activated biochar derived from *Anthriscus sylvestris,* which is characterized by high surface area, tailored pore structure, and abundant functional groups that enable various chemical and physical interactions with TET and CIPF. These surface properties help bridge the gap between low-cost biochars and more advanced adsorbents by achieving high removal efficiencies. In addition, this work clearly advances both the theoretical and practical understanding of adsorption kinetics by systematically comparing existing models, evaluating mechanism shifts, and providing robust parameters for process design. By combining batch and laboratory-scale fixed-bed column experiments, this work demonstrates the potential applicability and

scalability of ASBS for real-world wastewater treatment. Preliminary studies by our group have benchmarked ASBS against other locally available plant species in Finland, showing that *Anthriscus sylvestris* achieved higher removal efficiencies for TET and CIPF even in its raw form. While the use of plant-based biochar has been previously reported (Shirani et al., 2020, 2024), this is, to our knowledge, the first study employing ASBS in a dual-mode adsorption study for these pharmaceuticals, further highlighting its cost-effective and environmentally sustainable potential for application beyond laboratory scale.

2 Materials and Methods

2.1 Materials

In this study, analytical-grade chemicals and reagents were used. Tetracycline (TET) (CAS: 64–75-5), ciprofloxacin (CIPF) (CAS: 17850-5G-F) (assay: ≥ 98.0%), hydrochloric acid (37%) and sodium hydroxide (> 97%) were obtained from Sigma Aldrich. *Anthriscus sylvestris* was gathered from a local forest in Kuopio, Finland.

2.2 Preparation of Activated Biochar (ASBS)

Leaves of *A. sylvestris* were hand-picked, washed, and dried in the oven at 45 °C for 24 h. The dried leaves were ground and sieved through a 250 µm mesh screen. The sieved material was then placed in an oven, with the temperature increasing from ambient to 300 °C at a heating rate of 10 °C min^{-1}. The material remained at this temperature for approximately 15 min under nitrogen flow (1 L min^{-1}). These thermally treated samples were labeled "Inactivated Biochar" (INA-BC) (Fig. 1).

In this study, half of the INA-BC was chemically activated using NaOH. First, a mixture of INA-BC (3g) and 4 M NaOH (40 mL) was stirred for 2 h using a magnetic stirrer and allowed to be dried at 105 °C for 24 h. The material was thermally activated by heating from ambient temperature to 800 °C under nitrogen flow (2 L min^{-1}) at a rate of 3 °C min^{-1}, with a holding time of 2 h. The activation temperature (800 °C), time (2 h), and NaOH concentration (4 M) were chosen based on preliminary trials and previous studies to ensure sufficient surface area, pore volume, and functional group development (Wang et al., 2018; Mangla et al., 2022; Shirani et al., 2024). The activated sample was allowed to cool and then rinsed with 2 L of deionized water. Subsequently, it was treated with 200 mL of 0.1 M HCl for an acid rinse. The solids were further washed with deionized water until the pH of the filtrate became neutral, then dried at 50 °C for 24 h and named "Activated Biochar", (ASBS). Both INA-BC and ASBS were stored in sterilized, capped containers inside a desiccator for future use (Fig. 1). The final yield of activated biochar (ASBS) after chemical and thermal activation was calculated as the ratio of the final activated biochar weight (around 0.01 g) to the initial INA-BC used (3 g).

2.3 Characterization of ASBS

To examine the surface morphology of ASBS, an energy-dispersive X-ray analyzer was employed (Hitachi SU-8010, Japan). Surface functional groups, important in adsorption, were identified through Fourier Transform Infrared Spectroscopy (FTIR) using a Spectrum 100 spectrometer (PerkinElmer, Waltham, MA, USA).

2.4 Batch Adsorption Experiments

For this purpose, 0.1 g L^{-1} of ASBS was introduced into 15 mL polyethylene centrifuge tubes containing different concentrations of the adsorbates (10 to 100 mg L^{-1}). To investigate how the solution pH affects the adsorption of TET and CIPF, the pH was initially adjusted to 2, 4, 6, 8 and 10 using 0.1M HCl and 0.1M NaOH. Experimental conditions were optimized by examining various parameters, including ASBS dosage (0. 25–1.25 mg), agitation time (0–1600 min), initial adsorbate concentration (10–100 mg L^{-1}), temperature (−1, 25 and 35° C) and co-existing anions and cations at a natural pH of 5.17. For studying the effect of competing ions on TET and CIPF adsorption by ASBS, two concentrations of the co-existing ions (for TET: 50 and 100 mg L^{-1}, for CIPF: 25 and 50 mg L^{-1}) were added to the fixed pharmaceutical concentrations (100 mg L^{-1}: TET and 40 mg L^{-1}: CIPF). Throughout the experiments, a single parameter was modified, while the remaining variables were kept constant. All adsorption experiments were performed in duplicate, and the results are reported as arithmetic means with standard deviations below ± 5%. In each experiment,

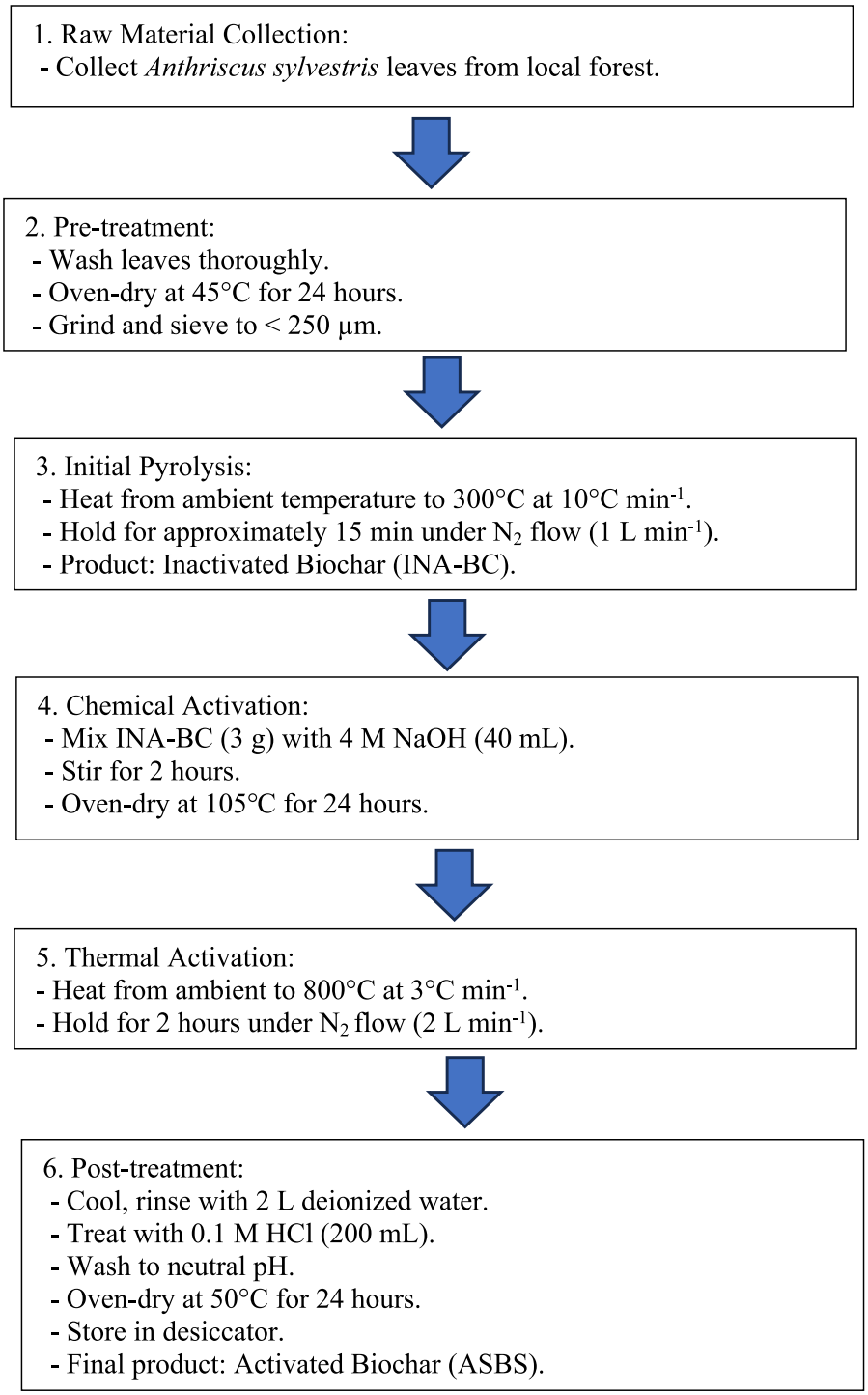

Fig. 1 Schematic representation of the chemical and thermal activation process for ASBS synthesis from *Anthriscus sylvestris*

the concentrations of adsorbates in stock solutions were measured before and after adsorption to assess any potential degradation and to verify mass balance, thereby confirming that the observed removal was due to adsorption rather than degradation losses. After each adsorption experiment, the supernatants were filtered using 0.42 µm cellulose nitrate membrane filter. The residual concentrations of TET and CIPF were then measured at maximum

wavelength of 357 (Tan et al., 2015) and 277 nm (Zeng et al., 2018), respectively using a UV spectrophotometer (Shimadzu corp. Tokyo, Japan). Prior to each set of measurements, the UV–Vis spectrophotometer was calibrated using standard solutions for TET and CIPF covering the full concentration range used in the experiments. The instrument's detection limit was approximately 0.01 mg L^{-1}, and potential interference from coexisting ions at measurement wavelengths was confirmed to be negligible.

The removal percentage and adsorption capacity of ASBS at equilibrium for TET and CIPF were calculated using Eqs. (1) and (2):

$$Removal\ percentage\% = \frac{(C_i - C_e)}{C_i} \times 100 \quad (1)$$

$$Adsorption\ capacity\left(mgg^{-1}\right) = \frac{V\left(C_i - C_e\right)}{W} \quad (2)$$

where, C_i is the initial concentration of TET or CIPF (mg L^{-1}) and C_e is the concentration of the TET or CIPF at equilibrium (mg L^{-1}), V is the volume of the TET or CIPF solution (mL) and W is the mass of ASBS (mg).

2.5 Determination of pH_{zpc}

To characterize the electrochemical properties of ASBS, pH drift method was used. The conducted method is explained in detail in our previous study (Shirani et al., 2020). After preparing a solution of 0.01 M NaCl, 0.01 g of ASBS was added to 5 mL of the solution while the initial pH of the solution was adjusted to 2, 4, 6, 8 and 10.

At the end of the experiment, the final pH (pH_f) of the supernatants was measured. To determine the pH at zero point of charge of ASBS, intersection of ΔpH against pH_i was plotted (Lopez-Ramon et al., 1999). ΔpH is expressed as the following Eq. (3):

$$\Delta pH = pH_{initial} - pH_{final} \quad (3)$$

2.6 Thermodynamic Studies

The adsorptive reaction orientation and feasibility were evaluated by calculating thermodynamic parameters, including Gibbs free energy (ΔG°), heat of adsorption (ΔH°), and entropy change (ΔS°), using the Eqs. (4) and (5):

$$\Delta G^\circ = -RT\ln K \quad (4)$$

$$\ln\left(\frac{q_e}{C_e}\right) = \frac{\Delta S^\circ}{R} - \frac{\Delta H^\circ}{RT} \quad (5)$$

where, T and R are known as the temperature (K or Kelvin) and the gas constant (8.314 J mol^{-1} K^{-1}), respectively.

2.7 Modeling of Adsorption Processes

2.7.1 Kinetic Modeling

Adsorption kinetics were investigated to examine the rate and dynamics involved in the adsorption process. Moreover, the results of these studies demonstrate the equilibration time for maximum uptake. The kinetic models applied in this study included: pseudo-first-order (PFO) and pseudo-second-order (PSO) models. PFO assumes that the occupation rate of the adsorbent's sorption sites by the adsorbate is proportional to the sites that are not yet occupied (Lagergren, 1898). PSO suggests that chemisorption limits the rate at which the adsorption process takes place and involves bonding forces through the exchange or sharing of electrons among the adsorbate molecules and the surface of the adsorbent (Ho & McKay, 1999). The non-linear form of PFO and PSO expressions are given by Eqs. (6) and (7):

$$q_t = q_e\left[1 - exp\left(-k_1 t\right)\right] \quad (6)$$

$$q_t = \frac{q_e^2 k_2 t}{1 + q_e k_2 t} \quad (7)$$

with k_1 and k_2 represent the rate constants, corresponding to the PFO (min^{-1}) and PSO (g mg^{-1} min^{-1}) models, respectively. The amount of TET or CIPF (mg g^{-1}) adsorbed at the equilibration time is q_e, at time t (min), the adsorbed quantity of TET or CIPF is q_t.

2.7.2 Isotherm Modeling

Adsorption isotherm studies are conducted to depict the adsorption mechanism of TET and CIPF by ASBS and to describe how the adsorbate interacts with the adsorbent. To describe the adsorption isotherms, four isotherm models were applied: Langmuir, Freundlich, Sips and Dubinin-Radushkevich. The Langmuir isotherm model describes adsorption occurring on homogenous surfaces with insignificant interaction between adsorbed molecules (Langmuir, 1918). The non-linear equation of this model is represented by Eq. (8):

$$q_e = \frac{q_m b C_e}{1 + b C_e} \tag{8}$$

where, q_e is considered the adsorbed amount of TET or CIPF by ASBS (mg g^{-1}) at equilibrium. The equilibrium concentration of TET or CIPF at equilibrium time and the constant of Langmuir are C_e (mg L^{-1}) and b (L mg^{-1}) respectively. The maximum adsorption capacity of TET and CIPF (mg g^{-1}) is q_m.

The Freundlich isotherm, an empirical model, describes multilayer adsorption on an adsorbent surface with heterogeneous properties (Freundlich, 1909) and is given by Eq. (9):

$$q_e = k_F C_e^{1/n} \tag{9}$$

where, q_e is the adsorbed amount of TET or CIPF using ASBS (mg g^{-1}) at equilibrium, C_e is the equilibrium concentration of TET or CIPF (mg L^{-1}) at equilibrium time and k_F is the constant (mg g^{-1}) (L $mg^{-1})^{1/n}$ of Freundlich.

The Sips model combines the Freundlich and Langmuir isotherm to predict heterogeneous adsorption systems while mitigating restriction of the Freundlich model. At low adsorbate concentrations, it follows the Freundlich isotherm model, whereas at higher concentrations it predicts the monolayer capacity of the Langmuir model (Sips, 1948). The Sips model parameters are affected by experimental conditions, including pH, temperature, and initial adsorbate concentrations (Sips, 1948). This model is demonstrated by Eq. (10):

$$q_e = \frac{q_m (k_S C_e)^m}{1 + (k_S + C_e)^m} \tag{10}$$

where, q_m is the maximum adsorption capacity of TET and CIPF at saturation (mg g^{-1}), k_S is the constant of sips isotherm model (L mg^{-1}), while m is considered as the exponent.

Dubinin-Radushkevich model is used to explain the adsorption mechanism occurring on heterogeneous as well as homogeneous surfaces (Dubinin & Radushkevich, 1947). One advantage of this model compared to other isotherm models is its consistency across different temperatures (Dubinin & Radushkevich, 1947). The non-linear form of this model is expressed by Eqs. (11) and (12) (Dubinin & Radushkevich, 1947):

$$q_e = q_m exp\left(-k_{DR}\mathcal{E}^2\right) \tag{11}$$

$$\mathcal{E} = RT\ln\left(1 + \frac{1}{C_e}\right) \tag{12}$$

where, q_e, q_m and k_{DR} are the theoretical adsorption capacity (mg g^{-1}), maximum sorption capacity of TET or CIPF adsorbed (mg g^{-1}) at the equilibrium and Dubinin-Radushkevich isotherm model constant (mol^2 J^{-2}), respectively. R stands for the universal gas constant (8.314 J K^{-1} mol^{-1}), and T represents the absolute temperature (K).

2.8 Fixed-Bed-Column Experiments

Fixed-bed-column studies were performed to obtain engineering data and to validate the potential of the material to be used for continuous, real-scale wastewater treatment (Bharathi & Ramesh, 2013). To carry out the column studies a glass column of 100 mm height, 6.6 mm internal diameter and 3400 mm^3 volume was used. The weight of ASBS was 0.025 g. Glass wool with the thickness of 0.04 cm in the top and bottom side of ASBS was used to provide mechanical support for the adsorbent and to prevent material loss and buoyancy. Flow rates were adjusted with a peristaltic pump. All experiments were conducted at room temperature (28 ± 1 °C). An assessment was made of the impact of flow rates (1 and 2 mL min^{-1} for both adsorbates) and different concentrations (TET concentrations ranged from 20 to 50 mg L^{-1}, and CIPF concentrations varied between 30 to 40 mg L^{-1}). These values were derived from typical TET concentrations found in liquid manure (Hamscher et al., 2002) and CIPF concentrations in

pharmaceutical effluents (Genç, 2015). Effluent Samples were collected at specific intervals and analysed using a UV-spectrophotometer to determine TET and CIPF concentration at 357 nm and 277 nm, respectively. Breakthrough curves were obtained by using the ratio of C/C_0 as a function of time. The breakthrough and saturation points correspond to effluent concentrations reaching 5% and 95% of C_0, respectively (Pérez-Morales et al., 2019). The empty bed contact time (EBCT) was calculated as the ratio of the column bed volume to the flow rate. Due to the small bed height and low flow rates used, any pressure drops across the packed bed was negligible.

3 Results and Discussion

3.1 Characterization

Anthriscus sylvestris was selected as a precursor for activated biochar due to its natural abundance, rapid growth, and local availability as an underutilized plant resource. The plant's lignocellulosic composition makes it suitable for producing carbon-rich material with a high degree of porosity and abundant surface functional groups after activation. These structural characteristics enhance the number of active sites available for adsorbing pharmaceutical molecules. *A. sylvestris* has not been widely studied for adsorptive applications; however, the biochar derived from this plant (ASBS) demonstrated promising physicochemical characteristics and high adsorption capacity, making it a strong candidate for pharmaceutical removal from water. The final yield of ASBS after chemical and thermal activation was approximately 0.33% of the INA-BC mass. Such a low yield is typical for strong alkali chemical activation, which removes ash and volatile matter, and creates a highly porous structure with abundant active sites for adsorption (Guo et al., 2024b).

3.1.1 SEM Analysis

The surface morphology of pristine plant material and the biochar before and after activation was examined using scanning electron microscope (SEM) (Fig. 2 (a)). Before activation, the external surfaces of the pristine plant and the inactivated biochar appeared smooth and mostly lacked pores (Fig. 2 (a) (i) and (ii)). After activation, numerous irregular and well-distributed pores appeared on the ASBS surface, visibly increasing its roughness and likely enhancing the accessible surface area for adsorption. This observation is consistent with recent findings, which showed that using strong bases such as NaOH as activating agents during lignin pyrolysis can produce carbon materials with exceptionally high BET surface area and pore volume, thus significantly boosting adsorption performance (Xu et al., 2024) (Fig. 2(a) (iii)). These porous structures may facilitate intraparticle diffusion and provide more active sites for the adsorption of TET and CIPF (Wang et al., 2022).

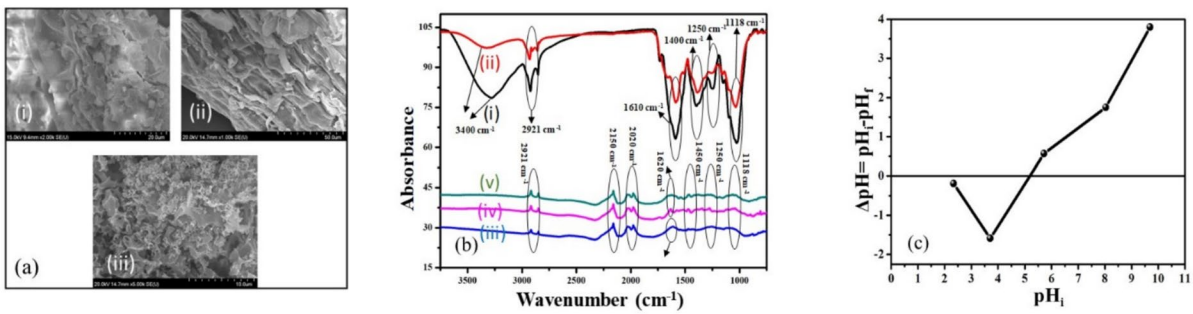

Fig. 2 (**a**) Scanning electron microscopy image of (i) *Anthriscus sylvestris*, (ii) INA-BC and (iii) ASBS and (**b**) FTIR spectra of (i) *Anthriscus sylvestris*, (ii) INA-BC and (iii) ASBS before and after adsorption of (iv) TET and (v) CIPF and (**c**) pH_{zpc} of ASBS (pH_i: initial pH of the solution & pH_f: final pH of the solution)

3.1.2 *Fourier Transform Infrared Spectroscopy (FTIR) Analysis*

The results from the FTIR spectra of the adsorbents (Fig. 2(b)) revealed the disappearance of several bands due to the activation process. This occurs because high temperatures partially decompose surface functional groups and release volatile matter (He et al., 2016). Both the pristine plant and INA-BC displayed a peak at 3400 cm^{-1} which can be attributed to O–H hydrogen bonding (He et al., 2016). The presence of a peak at 2921 cm^{-1} in both pristine plant and ASBS was attributed to aliphatic bonds (Pezoti et al., 2016; Wang et al., 2018). A peak at 1118 cm^{-1}, present in all samples before and after adsorption, may imply the stretching vibrations of C-O–H (He et al., 2016). The stretching vibration around 1400 cm^{-1} in both pristine plant and INA-BC could be attributed to highly conjugated C-O and C = O stretching of carboxylic groups (Pezoti et al., 2016). This peak shifted slightly to 1450 cm^{-1} in ASBS, suggesting that activation reduces oxygen-containing functional groups, enhancing adsorbate uptake (Taheran et al., 2016). After activation, the stretching vibration near 1250 cm^{-1}, assigned to C = O in the pristine plant, almost disappeared (He et al., 2016). The band observed near 1610 cm^{-1} was associated with the stretching of aromatic C = C bonds (Peng et al., 2015) in pristine plant, INA-BC, and ASBS, which shifted to 1620 cm^{-1} after the adsorption of TET and CIPF. This indicates that π-π electron donor–acceptor (EDA) interactions could significantly contribute to the adsorption of antibiotics onto the adsorbent (Zeng et al., 2018). In ASBS, stretching vibrations observed approximately at 2020 and 2150 cm^{-1} may be assigned to $C \equiv C$ and C = C, respectively (Mao et al., 2016; Ali et al., 2018).

Overall, the disappearance and shifts of oxygen-containing bands indicate a net reduction in acidic groups and relative enrichment of basic surface sites (Panwar & Pawar, 2022). This improves the hydrophilicity, aromaticity, and ion-exchange capacity of ASBS (Kumar et al., 2022). As a result, the modified surface can develop stronger electrostatic attractions and hydrogen bonds with the ionizable functional groups of TET and CIPF. Additionally, the preserved aromatic domains and the appearance of new C = C bonds support more pronounced π-π EDA interactions, further contributing to higher adsorption capacities. This improved surface chemistry, combined with the observed structural porosity, explains the increased adsorption capacity and efficiency of ASBS compared to the inactivated material.

The activation process not only removes ash and volatile matter but also promotes the formation of stable aromatic structures (e.g., C = C bonds), which increase the structural strength and stability of the adsorbent. This enhanced aromaticity and reduced impurities improve the material's adsorption efficiency and support its potential for regeneration and reuse without significant performance loss (Liu et al., 2021).

3.2 Effect of Solution pH

The acidity or basicity of the solution affects both the surface charge of the adsorbent and the ionization and the speciation of the adsorbate (Peng et al., 2015). Therefore, it is essential to determine the optimal pH by examining its effect on adsorption performance.

The pH at the zero point of charge (pH_{ZPC}) of the modified biochar was 5.17 (Fig. 2(c)), which is important when considering how TET and CIPF speciation varies with pH and affects electrostatic interactions during adsorption. TET is an amphoteric molecule (Wang et al., 2018; Fiori et al., 2022), consisting of three ionizable functional groups, including tricarbonyl methane, phenolic diketone and dimethylamine groups (Brinzila et al., 2012). It has three distinct pK_a values: 3.3, 7.8, and 9.6 (Martins et al., 2015; Oruganti et al., 2023). Thus, when the solution pH is lower than 3.3, the cationic H_4TC^+ form dominates. Zwitterionic species are predominant within the pH range of 3.3 to 7.8 (Martins et al., 2015). Anionic forms, such as TCH^- and TC^{2-} ions, dominate when the pH is higher than 9.6 (Fig. 3) (Wang et al., 2018).

As presented in Fig. 4(a) the adsorption of TET by ASBS showed clear pH dependence. At pH values below the pH_{zpc} (5.17), the surface of the ASBS is positively charged, leading to weaker π-π EDA interactions with the H_4TC^+ ions. However, increasing the pH to 4 enhances the adsorption due to stronger EDA interactions between the positively charged ASBS surface and the zwitterionic form of TET (Peiris et al., 2017). The π-π EDA interactions between antibiotics and carbonaceous materials might be considered as one of the most significant non-hydrophobic interactions (Liao et al., 2013). The benzene structure

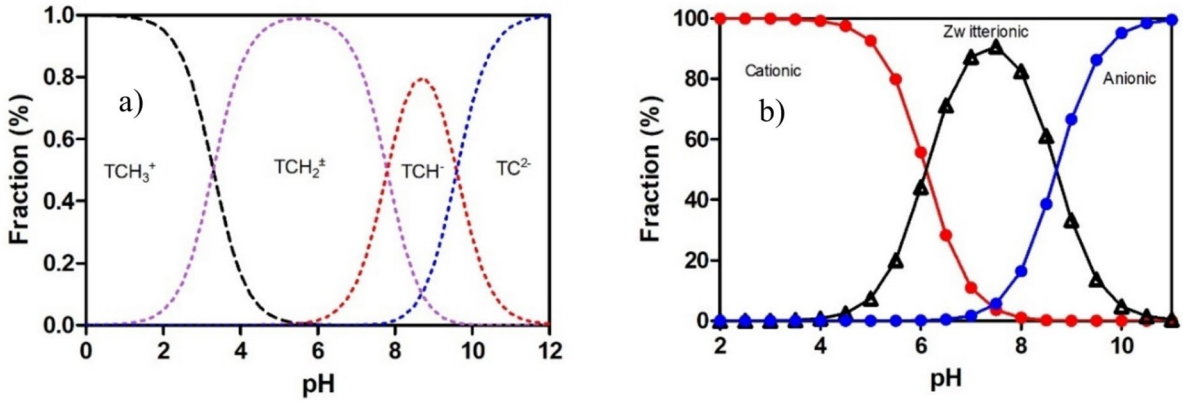

Fig. 3 Speciation diagram of (**a**) tetracycline (TET) and (**b**) ciprofloxacin (CIPF) as a function of pH indicating the various fractions

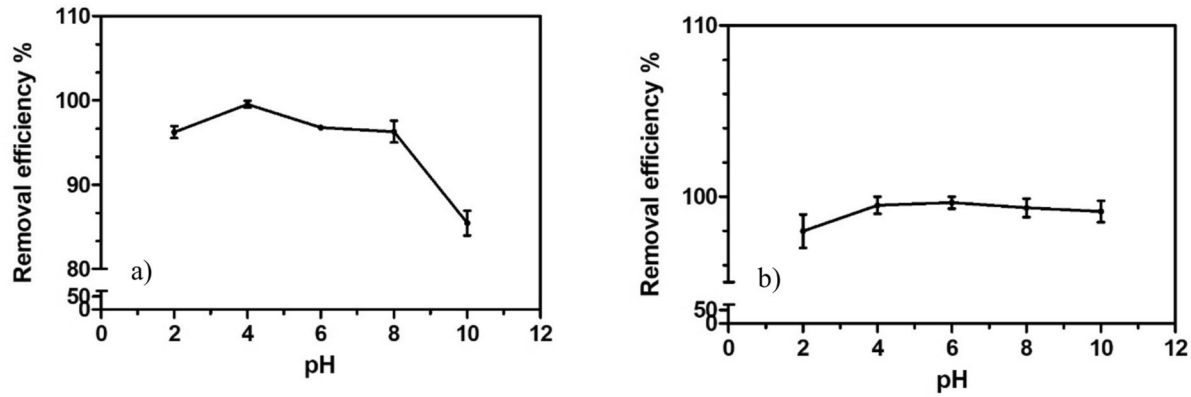

Fig. 4 (**a**) Effect of solution pH on TET and (**b**) effect of solution pH on CIPF removal using ASBS (Initial TET concentration: 50 mg L^{-1} and initial CIPF concentration of: 40 mg L^{-1}, dose of ASBS: 0.1 g $L.^{-1}$, in room temperature. All experiments were conducted in duplicate; error bars represent standard deviation)

of TET and the polarized aromatic rings of the adsorbent interact through the π-π EDA interactions (Liao et al., 2013). Additionally, non-specific van der Waals forces, H-bonding and hydrophobic interactions can contribute to TET adsorption at pH 4 (Martins et al., 2015; Zeng et al., 2019). H-bonding occurs through interactions between functional groups of TET, such as -OH, $-NH_2$, N–H and $-CH_3$, and the oxygen containing groups of ASBS, such as C-O–H (Liao et al., 2013). At pH values above 8, the surface of ASBS becomes negatively charged, leading to electrostatic repulsion with the anionic TET species (Peiris et al., 2017).

Furthermore, the impact of the pH level of the solution on the adsorption of CIPF by ASBS was studied across a pH range of 2–10. CIPF is an ionizable antibiotic with two pK_a values (6.1 and 8.7), so it can be present in positive, negative and zwitterionic forms (Li et al., 2014). For CIPF, the maximum adsorption capacity of 372.53 mg g^{-1} was obtained at natural pH (pH: 5.17) (Fig. 4(b)). Below pH 5.17 (pH_{zpc}), CIPF exists in its cationic form while ASBS is positively charged, resulting in electrostatic repulsion and a decrease in adsorption. Increased electrostatic attraction was observed in the pH range of 5.2–6.1 that can be due to different charges of CIPF molecules and ASBS surface (Li et al., 2014). When the pH of the solution is between 6.1 and 8.7, CIPF is in its zwitterionic form and its solubility is lowest, while its hydrophobicity is highest (Li et al.,

2014). This may explain the increased adsorption, as hydrophobic interactions play a key role in the adsorption of organic compounds (Peng et al., 2015). Above pH 8.7, both the ASBS and CIPF surfaces become negatively charged, and the concentration of OH^- ions increases, leading to a slight decrease in CIPF removal efficiency due to electrostatic repulsion (Yu et al., 2016) and competition with excessive OH^- ions (Dhiman & Sharma, 2018). Despite these factors, the removal efficiency of CIPF by ASBS remained high across the entire pH range (Fig. 4(b)). Therefore, subsequent adsorption studies were conducted using Milli-Q water (pH about 5.17).

3.3 Effect of the Adsorbent Dosage

Various ASBS dosages, ranging from 0.05 to 0.25 g L^{-1}, were tested for their effectiveness in adsorbing TET and CIPF. The adsorption of TET by ASBS increased from 51% to 99.9%, while that of CIPF sharply increased from 54.2% to 99.8% as the dose was raised from 0.05 to 0.25 g L^{-1} (Fig. 5(a) and (b)). The enhanced removal efficiency at higher doses may be attributed to an increase in an available adsorption surface area, active sites, and mass transfer driving forces (Shirani et al., 2018). However, the adsorption capacity of TET and CIPF by ASBS decreased from 521.55 to 204.71 and from 796.69 to 293.54 mg g^{-1}, respectively with an increase in ASBS dosage from 0.05 to 0.25 g L^{-1}. This reduction may occur due to agglomeration of biochar particles, which can lead to incomplete utilization of active sites for sorption (Ali et al., 2018).

3.4 Adsorption Kinetics

The adsorption kinetics of TET and CIPF onto ASBS were evaluated using PFO and PSO models at different initial concentrations. The amounts of TET (10 and 50 mg L^{-1}) and CIPF (10 and 40 mg L^{-1}) adsorbed by ASBS at different time intervals are illustrated in Fig. 6(a) and (b). The maximum adsorption of TET and CIPF was reached after 1400 and 380 min, respectively. The kinetic parameters for these models are summarized in Table 1. Additional detailed statistical indicators for the kinetic models, including chi-square (χ^2), residual sum of squares (RSS), and Akaike information criterion (AIC) values for each concentration and model, are provided in Tables S1 and S2 and the residual analysis are presented in Fig. S1 and S2.

For TET, the PSO model provided a better fit at 10 mg L^{-1}, with lower statistical error indicators (χ^2 = 1.97, RSS = 135.62, AIC = 30.07) and higher correlation (R^2 = 0.98) compared to the PFO model (χ^2 = 7.21, RSS = 395.25, AIC = 40.77, R^2 = 0.95) (Table S1). The PSO-predicted adsorption capacity (99.61 mg g^{-1}) was closer to the experimental value (103.11 mg g^{-1}) than the PFO prediction (96.90 mg g^{-1}), and the RMSE was significantly lower (3.85 vs. 6.62) (Table 1). At 50 mg L^{-1}, the PSO model again outperformed PFO, with χ^2 = 100.68, RSS =

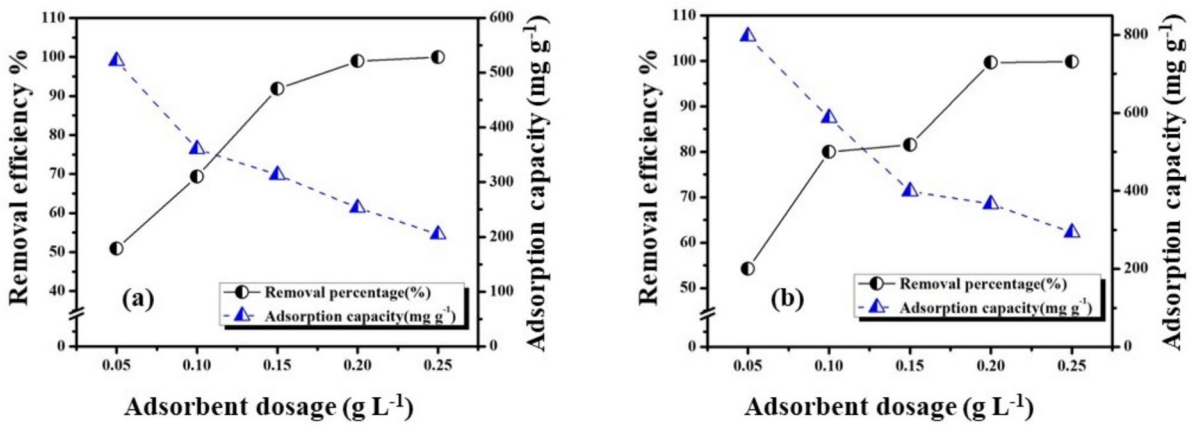

Fig. 5 (**a**) The impact of adsorbent dosage on TET and (**b**) the impact of adsorbent dosage on CIPF removal efficiency by ASBS (Concentration of TET: 50 and concentration of CIPF: 80 mg L.$^{-1}$)

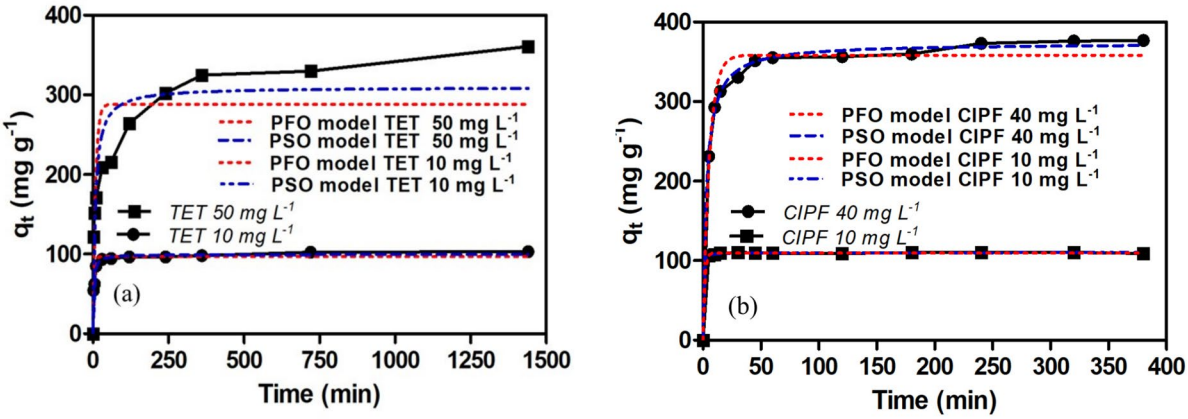

Fig. 6 (**a**) Kinetic Pseudo-first-order (PFO) and Pseudo-second-order (PSO) modelling of TET using ASBS (**b**) Kinetic PFO and PSO modelling of CIPF using ASBS

Table 1 Adsorption kinetic parameters for TET and CIPF on ASBS

Pharmaceutical	***Pseudo-first-order***				
	Experimental Adsorption Capacity (mg g^{-1})	Rate Constant (min^{-1})	Theoretical Adsorption Capacity (mg g^{-1})	Root Mean Squared Error (RMSE)	Coefficient of Determination (R^2)
TET 10 (mg L^{-1})	103.11	0.27	96.90	6.62	0.95
TET 50 (mg L^{-1})	360.91	0.11	288.3	52.18	0.79
CIPF 10 (mg L^{-1})	109.2	0.7	109.6	0.81	0.99
CIPF 40 (mg L^{-1})	376.87	0.18	358.3	17.59	0.99
Pharmaceutical	***Pseudo-second-order***				
	Experimental Adsorption Capacity (mg g^{-1})	Rate Constant(g mg^{-1} min^{-1})	Calculated Adsorption Capacity (mg g^{-1})	Root Mean Squared Error (RMSE)	Coefficient of Determination (R^2)
TET 10 (mg L^{-1})	103.11	0.0048	99.61	3.85	0.98
TET 50 (mg L^{-1})	360.91	0.0004	309.6	38.84	0.88
CIPF 10 (mg L^{-1})	109.2	0.053	110.1	0.60	0.77
CIPF 40 (mg L^{-1})	376.9	0.0009	373.4	6.48	0.99

13770.81, AIC = 76.28, and R^2 = 0.88, compared to higher errors for PFO (χ^2 = 150.53, RSS = 24601.28, AIC = 82.08, R^2 = 0.79) (Table S1). Moreover, from the residual plots (Fig. S1a-b) it was observed that the PSO model has a more random and symmetric distribution of residuals around zero, particularly at 10 mg L^{-1}, supporting the model's goodness-of-fit. These results suggest that chemisorption may play a dominant role in the adsorption mechanism of TET, especially at higher concentrations (Tan et al., 2015; Guo et al., 2024a, b).

For CIPF, a different trend was observed. At 10 mg L^{-1}, the PFO model exhibited better statistical performance, with lower χ^2 (0.64), RSS (70.6), and AIC (24.45) values and higher R^2 (0.99), closely matching the experimental adsorption capacity (109.6 mg g^{-1} vs. 109.2 mg g^{-1}) (Table 1 & S2). In contrast, the PSO model yielded higher χ^2 (1.35), RSS (147.2), and AIC (32.53), with a lower R^2 (0.77) (Table 1 & S2). The residual plots for this concentration (Fig. S2a-b) also supports this finding, as the PFO model displayed a more balanced and less patterned

residual distribution than the PSO model. However, at 40 mg L^{-1}, the PSO model performed better (χ^2 = 151.99, RSS = 43858.47, AIC = 95.20, R^2 = 0.9979) than PFO (χ^2 = 176.43, RSS = 47108.97, AIC = 97.12, R^2 = 0.9962), and its predicted adsorption capacity (373.4 mg g^{-1}) more closely approximated the experimental value (376.87 mg g^{-1}) (Table 1 & S2). Corresponding residual plots at 40 mg L^{-1} (Fig. S2c-d) revealed that the PSO model had slightly less systematic error and more randomly scattered residuals compared to the PFO model, supporting its reliability at higher concentrations.

These findings suggest a possible concentration-dependent shift in the adsorption mechanism. The PFO model fits better at lower CIPF concentrations, indicating a predominantly physisorption-driven process. While the PSO model provides better fits at higher concentrations for both TET and CIPF, suggesting a transition toward intraparticle diffusion and stronger surface interactions such as chemisorption, aligning with the PSO model assumptions. These likely involve electron exchange or sharing between the adsorbate and functional groups on the ASBS surface (Peiris et al., 2017; Das et al., 2018). These interactions may occur between the adsorbates and functional groups on the ASBS surface, including amino groups and accessible adsorption sites (Shirani et al., 2018). The shift from PFO to PSO dominance suggests that the rate-limiting step may change from boundary layer diffusion at low concentrations to surface reaction and pore diffusion at higher loadings (Mohamed Nasser et al., 2024), further supporting the complex adsorption mechanism of ASBS. The dominance of the PSO model indicates that chemisorption is likely the rate-limiting step, suggesting stronger and more stable adsorbate-adsorbent interactions. This behaviour is highly advantageous for practical applications in large-scale and continuous flow systems, where competing ions and fluctuating operating conditions can otherwise lead to desorption and reduced treatment efficiency (Tan et al., 2015). However, the observed decrease in the PSO rate constant (k^2) with increasing initial concentrations of TET and CIPF can be attributed to higher surface loading and intensified competition for active sites, which reduce diffusion efficiency and slow down the adsorption rate (Sayğılı & Güzel, 2016).

3.5 Adsorption Isotherms

Representative Langmuir (Eq. 8), Freundlich (Eq. 9), Sips (Eq. 10) and Dubinin-Radushkevich (Eqs. 11 and 12) adsorption isotherm models were applied to batch experiments where, 0.1 g L^{-1} of ASBS and 10–100 mg L^{-1} of TET and CIPF solutions were prepared. These four isotherm models were chosen to comprehensively describe different possible adsorption behaviours: Langmuir (monolayer, homogeneous), Freundlich (multilayer, heterogeneous), Sips (hybrid), and Dubinin-Radushkevich (energy and pore-filling insight).

The equilibrium adsorption data and their fits to these models are presented in Fig. 7(a) and (b) for TET and CIPF, respectively. These plots show how well each model describes the experimental data across the studied concentration range.

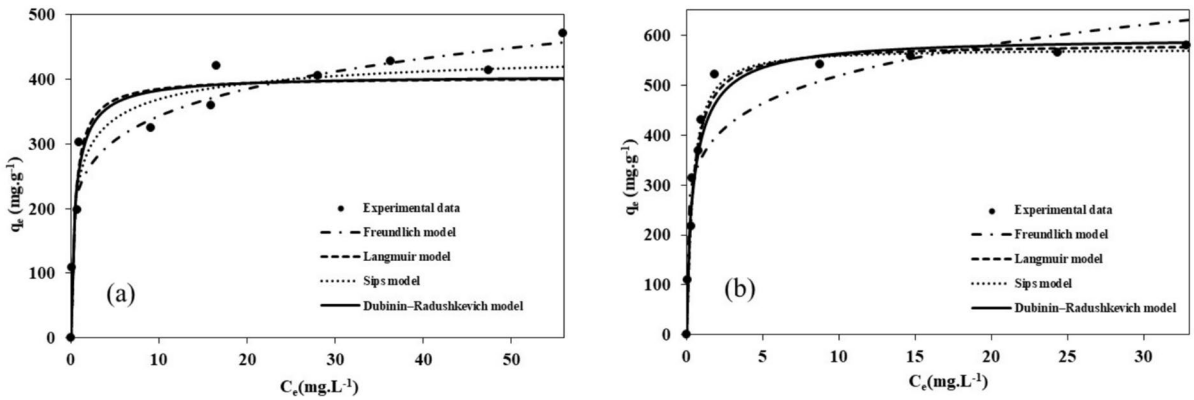

Fig. 7 (**a**) Freundlich, Langmuir, Sips and Dubinin-Radushkevich Isotherm modeling of TET and (**b**) CIPF using ASBS

Although all four models showed reasonable R^2 values ($R^2 \geq 0.93$) (Table 2), further evaluation using residual analysis (Fig. S3-S4), chi-square, RSS and AIC (Tables S3-S4) revealed deeper insight into the model performance and fitting quality.

The Langmuir model estimated the maximum adsorption capacities as 402.7 mg g^{-1} for TET and 582.2 mg g^{-1} for CIPF. As the experimental data of TET can be modelled using both Langmuir and Freundlich ($R^2 = 0.97$), adsorption appears to involve not only monolayer coverage but also occurs on a heterogeneous surface. Other studies have also reported the possibility of simultaneous interactions during the adsorption process (Wang et al., 2010; Liu et al., 2012). However, based on residual analysis (Fig. S3), chi-square, and AIC values, the Sips model provided the best statistical fit to the experimental data, indicating that the adsorption process may also involve a hybrid mechanism that combines features of both Langmuir and Freundlich models. This is supported by the lowest χ^2 (33.92), RSS (9520.79), and AIC (74.59) among all models (Table S3). In contrast, the Dubinin-Radushkevich model showed the poorest fit, with a significantly higher chi-square ($\chi^2 = 1548.85$) and AIC value (Table S3). This suggests that micropore-filling was not the dominant mechanism and that the ASBS material likely has a heterogeneous surface with varied pore structures. These results indicate that the adsorption of TET on ASBS may initially occur on a heterogeneous surface and gradually approach monolayer coverage as concentration increases, supporting the hybrid features of the material. For CIPF, Langmuir coefficient (0.99) was higher than Freundlich coefficient (0.93), and its b constant value was low, indicating monolayer adsorption with moderate binding affinity (Sayğılı & Güzel, 2016). Residual plots in Fig. S4 showed that Langmuir and Sips models produced more evenly distributed residuals compared to Freundlich and Dubinin-Radushkevich, which had broader dispersion and systematic deviation. The Langmuir model exhibited the lowest statistical error values ($\chi^2 = 12.02$, RSS = 4238.03, AIC = 64.49) and therefore, was selected as the most appropriate model for CIPF adsorption, despite the Sips model showing a slightly lower AIC (64.39) due to its interpretability and theoretical simplicity and favourability in practical applications (Swenson & Stadie, 2019). In contrast, the Freundlich model retained a much higher error level ($\chi^2 = 159.59$), confirming that the system does not follow a multilayer adsorption mechanism. Moreover, the Freundlich exponent was below 1 for both TET and CIPF, suggesting weak interaction energies between adsorbent and adsorbate (Peiris et al., 2017). The Dubinin-Radushkevich equation results showed that energy of TET and CIPF adsorption on ASBS were 1.42 and 1.44 kJ mol^{-1}, respectively, suggesting a physical adsorption process. However, poor statistical indicators limit the suitability of this model.

Table 2 Adsorption isotherm data for TET and CIPF on ASBS

Pharmaceutical	***Langmuir***			
	q_m (mg g^{-1})	b (L mg^{-1})	RMSE	R^2
TET	402.75	2.11	31.35	0.97
CIPF	582.18	2.50	21.70	0.99
Pharmaceutical	***Freundlich***			
	k_F (mg g^{-1}) (L mg^{-1})$^{1/n}$	1/n	RMSE	R^2
TET	233.86	0.16	32.18	0.97
CIPF	356.17	0.16	75.06	0.93
Pharmaceutical	***Sips***			
	q_m (mg g^{-1})	k_S (L mg^{-1})	n	R^2
TET	461.73	1.17	1.87	0.95
CIPF	572.67	2.91	0.86	0.98
Pharmaceutical	***Dubinin-Radushkevich***			
	q_m (mg g^{-1})	b	E	R^2
TET	405.73	0.24	1.42	0.95
CIPF	595.28	0.23	1.44	0.98

Therefore, these results emphasize the value of residual analysis in selecting the model and reinforce that the Sips model is the most suitable for describing TET adsorption, while the Langmuir model best described CIPF adsorption, supported by both fit quality and model simplicity.

Different adsorbents have various adsorption capacities for removal of TET and CIPF (Tables 3 and 4). For TET, its capacity (402.75 mg g^{-1}) exceeds that of activated carbon from tyre pyrolysis char (356 mg g^{-1}) (Acosta et al., 2016) and is significantly higher than typical biochars such as rice straw biochar (13.2 mg g^{-1}) (Wang et al., 2018) and also commercial activated carbon (28.6 mg g^{-1}) (Selmi et al., 2018). For CIPF, ASBS achieves 582.18 mg g^{-1}, comparable to high-performance modified biochars (e.g., LDO modified biochar, 744 mg g^{-1}) (Yu et al., 2025) and higher than multi-walled carbon nanotubes (150–205 mg g^{-1}) (Yu et al., 2016) and commercial activated carbon (71.9 mg g^{-1}) (Peñafiel et al., 2021). These results demonstrate that ASBS has higher adsorption capacity compared to most other adsorbents, likely due to its porosity and functional groups.

Table 3 TET removal efficiencies of different adsorbents

Adsorbent	Adsorption capacity (mg g^{-1})	References
Pumic stone	20.0	(Guler & Sarioglu, 2014)
Porous carbon from cellulose	1072.8	(He et al., 2016)
NaOH-activated carbon prepared via macadamia nut shells	490.0	(Martins et al., 2015)
Activated carbon from tyre pyrolysis char	356.0	(Acosta et al., 2016)
Activated carbon from tomato	500.0	(Sayğılı & Güzel, 2016)
Biochar from rice straw	13.2	(Wang et al., 2018)
Biochar from swine manure	8.1	(Wang et al., 2018)
Bamboo charcoal	22.7	(Liao et al., 2013)
Biochar from fast pyrolysis of biomass	58.8	(Liu et al., 2012)
Engineered hydrochar	47.0	(Jeganathan et al., 2024)
Engineered biochar	41.7	(Jeganathan et al., 2024)
Commercial activated carbon	28.6	(Selmi et al., 2018)
ASBS	402.75	***Present study***

Table 4 CIPF removal efficiencies of different adsorbents

Adsorbent	Adsorption capacity (mg g^{-1})	References
Bamboo-based carbon	233.3	(Peng et al., 2015)
Modified mesoporous carbon	362.9	(Peng et al., 2015)
Multi-walled carbon nanotubes	150.6–205.0	(Yu et al., 2016)
Rice straw biochar	76.6	(Zeng et al., 2018)
Porous Graphene Hydrogel	235.6	(Ma et al., 2015)
Magnetic Carbon composite	90.1	(Mao et al., 2016)
Activated carbon from lignin with H_3PO_4 activation	418.6	(Huang et al., 2014)
LDO modified biochar	744.0	(Yu et al., 2025)
Commercial activated carbon	71.9	(Peñafiel et al., 2021)
ASBS	582.18	***Present study***

3.5.1 *Benefits of ASBS Compared to Activated Carbon*

On average, preparing activated carbon and biochar costs approximately US$1500/t and US$ 246/t, respectively (Shirani et al., 2020). Therefore, producing biochar is more economically feasible in comparison to commercial activated carbon, especially due to the use of inexpensive raw materials and readily available activation methods. It would be beneficial for future studies to thoroughly analyze the cost–benefit aspects of ASBS, to evaluate its potential use in wastewater treatment plants. Since ASBS is derived from indigenous plants and activated with non-toxic, affordable chemicals, it offers a cost-effective alternative to conventional activated carbon.

Moreover, to determine the true cost-effectiveness of ASBS, regeneration studies should be conducted in future. However, given the availability and abundance of raw materials, as well as the additional preparation steps required for reusing exhausted biochar (e.g., acidic, alkaline, or thermal treatments), it may be more practical in some cases to consider fresh biochar rather than regenerating used material (Inyang & Dickenson, 2015). Additional studies are recommended to confirm this finding.

3.6 Effect of Temperature

To gain further insight into the adsorption mechanisms of TET and CIPF removal by ASBS, thermodynamic parameters were calculated at different temperatures (−1, 25 and 35 °C at pH 5.17) (Table 5).

For both TET and CIPF, ΔG° values were negative at all temperatures, indicating that the adsorption process was thermodynamically spontaneous. The ΔG° for TET ranged from −30.33 to −35.56 kJ mol^{-1}, and for CIPF from −32.95 to −44.66 kJ mol^{-1}, with more negative values observed at higher temperatures, suggesting greater spontaneity with increasing temperature. Similar thermodynamic results have been reported previously (Acosta et al., 2016; He et al., 2016; Wang et al., 2018). The ΔH° values were positive for both adsorbates, at +4.32 kJ mol^{-1} for TET and +9.66 kJ mol^{-1} for CIPF, verifying that the adsorption process is endothermic (Bazkiaee et al., 2024; Sharma et al., 2024). These enthalpy values are relatively low (< 40 kJ mol^{-1}), which typically corresponds to physical adsorption mechanisms involving weak interactions such as van der Waals forces or hydrogen bonding (Nasir et al., 2025). Similarly, the positive ΔS° values (0.05 J mol^{-1} K^{-1} for TET and 0.04 J mol^{-1} K^{-1} for CIPF) indicate increased randomness at the solid-solution interface, possibly due to structural reorganization of water molecules and release of adsorbed solvent during adsorption (Guler & Sarioglu, 2014; He et al., 2016).

The thermodynamic results suggest that the adsorption of TET and CIPF onto ASBS involves a combination of physical and chemical interactions. The low enthalpy changes (< 40 kJ mol^{-1}) and modest entropy values are consistent with physisorption processes such as van der Waals forces or hydrogen bonding. However, the highly negative Gibbs free energy values (−30 to −44 kJ mol^{-1}), along with the presence of surface functional groups, imply that chemisorptive interactions may also be involved. These findings highlight the complex nature of the adsorption mechanism, where both physisorption and chemisorptive interactions may occur simultaneously, depending on concentration and availability of functional groups (Ali et al., 2024). This mixed adsorption mechanism suggests that ASBS could potentially be regenerated and reused multiple times using relatively mild desorption processes, since physisorption is typically reversible and does not significantly degrade the adsorbent surface. Moreover, the endothermic nature of the process implies that adsorption efficiency may improve at the slightly elevated temperatures commonly found in real wastewater treatment plants (Wilson & Worrall, 2021). This supports the practical viability of ASBS under operational conditions.

3.7 Effect of Competing Anions and Cations

Since competing ions such as K^+, Na^+ and SO_4^{2-} are present in real wastewater, they are crucial factors influencing the adsorption of pharmaceuticals such as TET and CIPF. Figure 8 illustrates the impact of competing ions on the removal efficiency of these pharmaceuticals using ASBS. Subfigure 8(a) shows the impact of competing anions, while 8 (b) highlights the effect of competing cations on TET removal. Similarly, the effect of anions and cations on CIPF removal are presented in Fig. 8(c), and 8 (d), respectively. For this purpose, two initial concentrations of the competing ions were selected. The study

Table 5 Thermodynamic parameters for the adsorption of TET and CIPF onto ASBS

Parameter Adsorbate	Temperature (K)	Equilibrium Constant (L mol^{-1})	Gibbs Free Energy (ΔG) (kJ mol^{-1})	Entropy Change (J $(mol\ K)^{-1}$)	Enthalpy Change (kJ mol^{-1})
TET	272.15	33.60	−30.33	0.05	4.32
	298.15	41.29	−34.29		
	308.15	43.22	−35.56		
CIPF	272.15	164.30	−32.95	0.04	9.66
	298.15	461.10	−39.27		
	308.15	2261.63	−44.66		

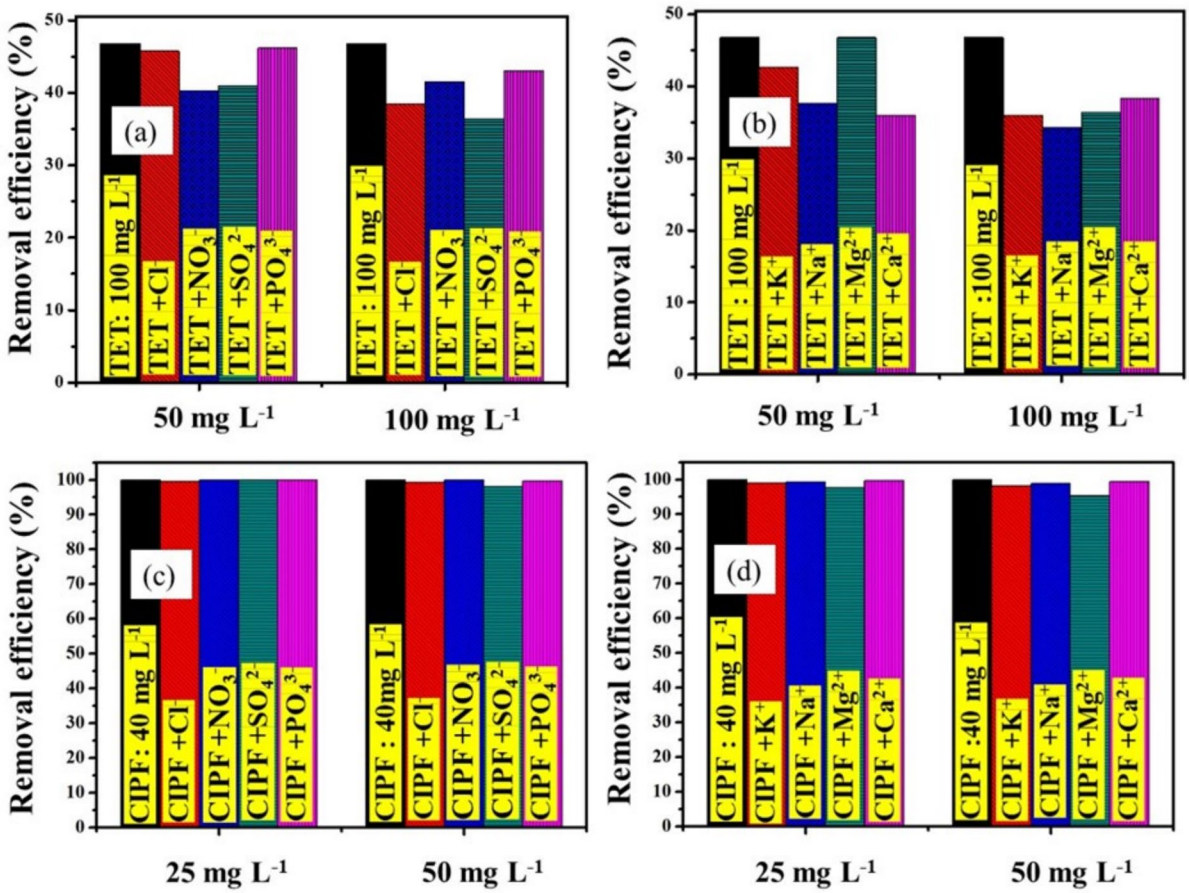

Fig. 8 Impact of competing (**a**) & (**b**) anions and cations on TET removal, respectively and (**c**) & (**d**) anions and cations on CIPF removal, respectively by ASBS (For TET the initial concentration is: 100 mg L^{-1} and for CIPF it is: 40 mg L^{-1}, dose of ASBS: 0.1 g $L.^{-1}$, in room temperature)

considered the effect of monovalent cations (K^+ and Na^+), divalent cations (Ca^{2+} and Mg^{2+}), monovalent anions (Cl^-, NO_3^-), divalent anions (SO_4^{2-}) and trivalent anions (PO_4^{3-}). All experiments were conducted at a pH of approximately 5.17. At this pH, the ASBS surface is negatively charged, while TET is mainly present as zwitterion and tends to aggregate in solution. Divalent metals, such as Ca^{2+} and Mg^{2+},

increase this aggregation, and due to cosolvent solubilization, the solubility of TET may increase, which can reduce its sorption capacity (Peiris et al., 2017).

As shown in Fig. 8(a) and (b), both anions and cations had negative effects on TET adsorption. At the higher competing ion concentration tested (100 mg L^{-1}), TET removal decreased by up to 27% in the presence of Na^+, Mg^{2+} and Ca^{2+}, while SO_4^{2-}caused a reduction of approximately 22% compared to the control. This may be due to the electrostatic screening effect that occurs at high ionic concentrations (Tan et al., 2015; Peiris et al., 2017). Such screening decreases the sorption capacity of TET, as ions such as Cl^- and Na^+ can be located near the adsorbent's carbon surface and interact with the partially ionized TET molecules (Rivera-Utrilla et al., 2013). Additionally, Na^+ can occupy available adsorption sites, further decreasing the adsorption of TET (Tan et al., 2016).

Similarly, the effect of competing anion and cations on CIPF removal are illustrated in Fig. 8(c) and (d), respectively. CIPF removal was only slightly impacted by the competing ions, as there was no considerable competition between CIPF and other ions for the adsorption sites. The presence of Mg^{2+} resulted in the greatest decrease for CIPF removal, by up to approximately 4.7%, while anions had a minimal effect (< 2% loss), even at 50 mg L^{-1} competing ion concentration. The negative effect of Ca^{2+} and Mg^{2+} on CIPF adsorption might be due to complex formation, which alters CIPF's atomic charge distribution and molecular orbitals, thereby stabilizing it in solution (Sun et al., 2018). Overall, the modest impact of competing ions on CIPF removal suggests that ASBS retains its adsorption efficiency under conditions similar to real wastewater, where multiple ions coexist. This emphasizes the importance of adsorbent selectivity, as also demonstrated by recent studies on functionalized biochars (Lu et al., 2025) which show that maintaining adsorption capacity despite ionic competition is essential for effective large-scale wastewater treatment.

These findings can be explained mechanistically by considering how ionic strength influences the biochar surface charge and the electrical double layer. Higher ionic strength compresses the electrical double layer around the adsorbent, which screens and neutralizes surface charges, thus weakening electrostatic interactions with pharmaceutical species (Zhang et al., 2019; Liu et al., 2022). Future studies should investigate the effects of different ion concentrations and other competing ions under realistic wastewater conditions.

3.8 Fixed-bed Column Experiments

To evaluate the performance of ASBS under continuous flow conditions, adsorption studies were conducted using a fixed-bed column setup. The effects of various adsorbate concentrations and flow rates on the breakthrough curves were investigated.

3.8.1 Impact of TET and CIPF Concentration

The relationship between the initial TET and CIPF concentrations was examined at different starting concentrations (TET: 20 and 50 mg L^{-1}; and CIPF: 30 and 40 mg L^{-1}) with a bed mass of 0.025 g and flow rates of 2 and 1mL min^{-1} for TET and CIPF, respectively.

As illustrated in Fig. 9(a) and (c), higher initial concentrations of TET and CIPF lead to a faster breakthrough and saturation compared to lower concentrations. For TET, an increase in concentration from 20 to 50 mg L^{-1} reduced the breakthrough time from 2.5 to 1 min, with equilibrium achieved after 480 and 450 min, respectively. Similarly, increasing the CIPF concentration from 30 to 40 mg L^{-1} decreased the breakthrough time from 10 to 2.5 min, with equilibrium reached after 230 and 190 min, respectively. Higher concentrations lead to more rapid saturation of the available binding sites as a result of lower mass transfer resistance and higher concentration gradients (Nazari et al., 2016; Shirani et al., 2018). Previous studies have also investigated the effect of lower adsorbate concentrations on breakthrough behavior (Shirani et al., 2024).

The Yoon-Nelson model was applied to predict the dynamic behaviour of TET and CIPF breakthrough in the column. As the initial concentration of TET increased from 20 to 50 mg L^{-1} (at 2 mL min^{-1}), the rate constant (k_{YN}) slightly increased from 0.0048 to 0.0056 min^{-1}, while the time required for 50% breakthrough (τ) significantly decreased from 113.31 to 31.96 min. Similarly, for CIPF, increasing the concentration from 30 to 40 mg L^{-1} (at 1 mL min^{-1}) led to a decrease in τ from 114.26 to 75.84 min and a reduction in k_{YN} from 0.0309 to

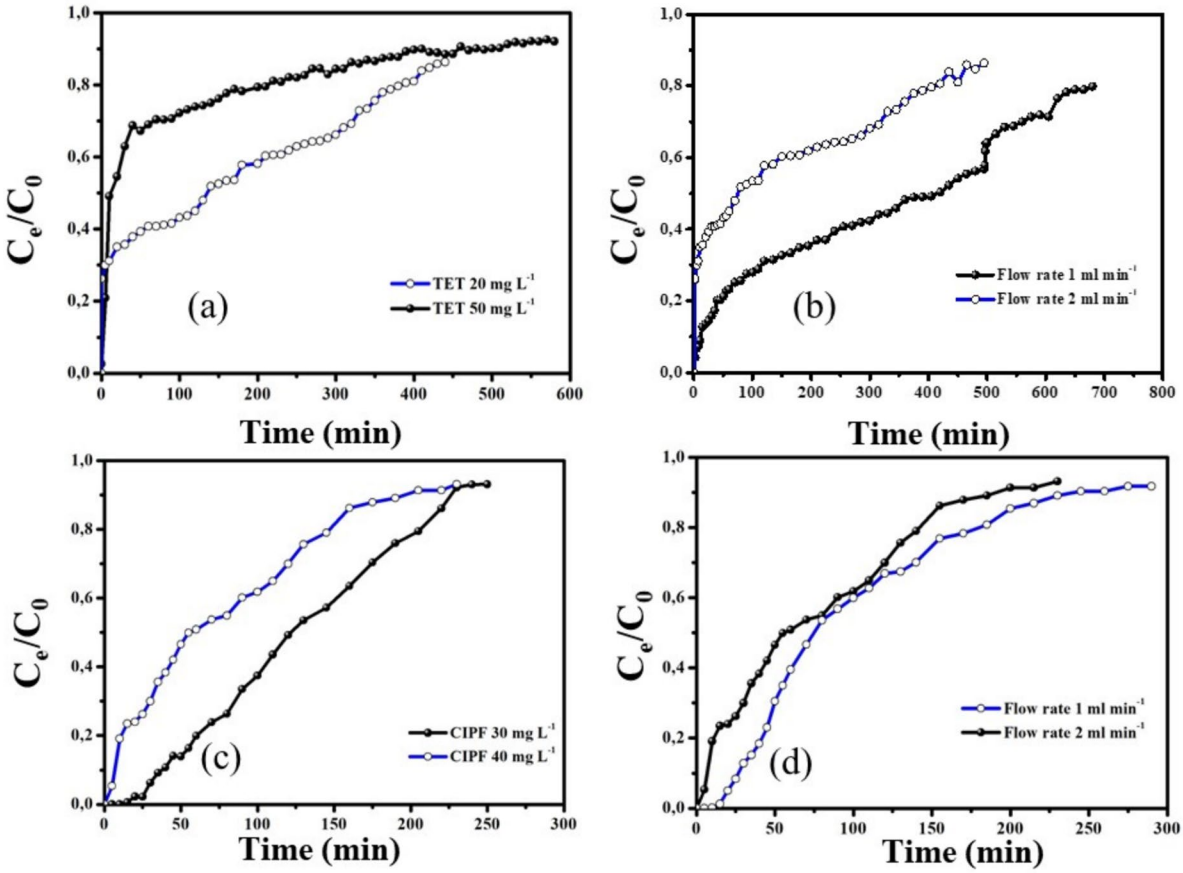

Fig. 9 Breakthrough curve of TET as function of (**a**) TET concentration (**b**) Flow rate and Breakthrough curve of CIPF as function of (**c**) CIPF concentration and (**d**) Flow rate (The initial concentration of the adsorbate: 10 mg L^{-1}, dose of ASBS: 0.25 g $L.^{-1}$, pH: normal)

Table 6 Yoon-Nelson Model Parameters for TET and CIPF Adsorption in Fixed-Bed Column Studies

Pharmaceutical	Concentration (mg L^{-1})	Flow rate (ml min^{-1})	k_{YN} (min^{-1})	τ (min)	R^2
TET	20	1	0.0530	38.82	0.94
	20	2	0.0048	113.31	0.96
	50	2	0.0056	31.96	0.81
CIPF	30	1	0.0309	114.26	0.94
	30	2	0.0252	137.62	0.89
	40	1	0.0190	75.84	0.93

0.0190 min^{-1} (Table 6 and Fig. S5.). These findings support the visual trends observed in Fig. 9a and c, indicating that higher initial concentrations result in faster saturation of adsorption sites.

3.8.2 Impact of Flow Rate

The column studies were performed at various flow rates (1 and 2 mL min^{-1}) with a constant bed height of

1 cm, (bed volume = 0.34 cm^3; bulk density = 0.073 g cm^{-3}), to determine the optimal contact time between adsorbent and adsorbate. The empty bed contact time (EBCT) was approximately 0.34 min for 1 mL min^{-1} and 0.17 min for 2 mL min^{-1}. The shorter EBCT at higher flow rates explains the faster breakthrough observed, as the contact time between the adsorbate and ASBS is reduced.

For determining the breakthrough curve, the ratio of C_e/C_0 was plotted against time. Higher flow rates led to earlier breakthroughs (Fig. 9(b) and (d)). When the flow rate was maintained at 1 mL min^{-1}, the observed breakthrough times were 3 min for TET and 5 min for CIPF. After increasing the flow rate to 2 mL min^{-1}, shorter breakthrough times were recorded (1 min for TET and 2.5 min for CIPF). This is likely due to the reduced residence time, which may prevent adequate contact between the adsorbates (TET and CIPF) and the adsorbent. Moreover, at higher flow rates, there is insufficient time for the adsorbates to diffuse into the pores of ASBS, causing TET and CIPF to pass through the column before equilibrium is reached. Similar results on the effect of higher flow rates on equilibrium have been reported in previous studies (Jahangiri-Rad et al., 2014).

As shown in Fig. 9(b) and (d), increasing the flow rate from 1 to 2 mL min^{-1} decreased the total amount adsorbed for both TET and CIPF. Similar results have indicated that higher flow rates lead to lower adsorption amounts (Liao et al., 2013; Nazari et al., 2016). Therefore, lower flow rates are more favorable for the adsorption of TET and CIPF, resulting in higher removal efficiencies.

According to the Yoon-Nelson parameters, an increase in flow rate from 1 to 2 mL min^{-1} led to a significant increase in τ for TET (from 38.82 to 113.31 min), despite a sharp decline in k_{YN} from 0.053 to 0.0048 min^{-1}, indicating a slower adsorption rate and a faster approach to 50% breakthrough. For CIPF at 30 mg L^{-1}, a similar trend was seen where increasing the flow rate reduced k_{YN} from 0.0309 to 0.0252 min^{-1} and increased τ from 114.26 to 137.62 min (Table 6, Fig. S6). These results confirm that higher flow rates reduce the adsorption rate by limiting the contact time and equilibrium attainment, consistent with the observed breakthrough curves in Fig. 9b and d. Overall, the Yoon-Nelson model parameters demonstrate good agreement with the experimental data and provide a predictive basis for estimating column performance under different flow conditions.

These findings suggest that maintaining an adequate empty bed contact time (EBCT) is important for efficient removal of TET and CIPF under continuous operation and real conditions. The observed effects of flow rate and initial concentrations indicate that lower flow rates and moderate loading concentrations are preferable for full-scale systems to maximize the adsorption efficiency and bed utilization. The fitted Yoon-Nelson parameters provide a basis for predicting the column performance under varying operating conditions. This information can be used to design larger fixed-bed systems with appropriate bed depth, flow distribution, and regeneration intervals. For practical application, pilot-scale or field-scale experiments should be conducted to validate these model predictions and refine design parameters accordingly.

3.9 Mechanism of TET and CIPF Adsorption using ASBS

The adsorption mechanism of TET and CIPF onto ASBS involves multiple interactions. At a pH of approximately 5.17, the negatively charged surface of ASBS favors electrostatic interactions with the zwitterionic form of TET and the cationic form of CIPF, resulting in faster and higher adsorption of CIPF. FTIR spectra before and after adsorption show shifts in -OH, C = O, and aromatic C = C stretching bands, confirming the contributions of hydrogen bonding and π-π EDA interactions. The benzene rings in the molecular structures of TET and CIPF enable π-π EDA interactions with the polarized graphite structure of the adsorbent (Ji et al., 2011). The electron-withdrawing ability of TET is stronger than that of CIPF due to the presence of nitro and ketone groups, allowing stronger π-π EDA interactions with the π-electron-rich graphite surfaces of ASBS (Ma et al., 2015). In addition, both antibiotics contain polar functional groups, such as hydroxyl (-OH), phenol, and amine ($-NH_2$), which can form hydrogen bonds with functional groups on the ASBS surface (e.g., C = O and -COOH). The N–H, -OH, and $-CH_3$ groups on ASBS can serve as hydrogen bond donors or acceptors, facilitating these interactions. TET, in particular, forms multiple hydrogen bonds with ASBS due to its several hydroxyl groups, enhancing its adsorption capacity (Liao et al., 2013; Tong et al., 2019).

Cation-π interactions may also contribute to the adsorption of both TET and CIPF on ASBS. These interpretations align well with previously reported adsorption mechanisms for carbonaceous adsorbents interacting with TET and CIPF, where similar π-π, hydrogen bonding, and electrostatic interactions have been confirmed (Biswal & Balasubramanian, 2022; Ajala et al., 2023; Álvarez-Torrellas et al., 2024). The possible sorption mechanism for the removal of TET and CIPF using ASBS is illustrated in Fig. 10. These findings suggest that ASBS is effective in removing both amphoteric compounds (e.g. TET) and ionic compounds (e.g. CIPF).

3.9.1 *Limitations of this Study*

This work revealed promising results in adsorption of pharmaceuticals using locally available biomass. However,

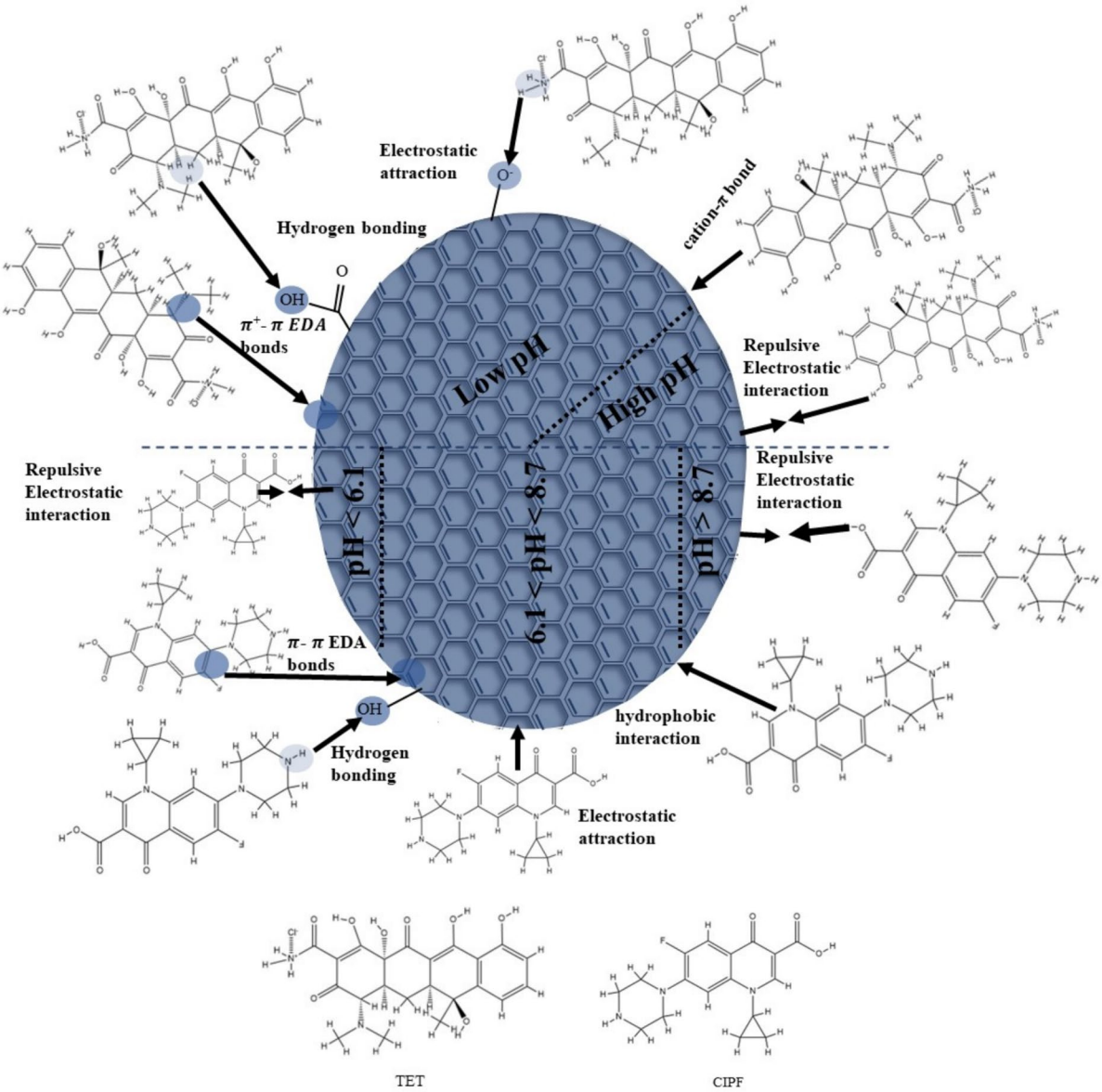

Fig. 10 Proposed sorption mechanism for the removal of TET and CIPF by ASBS (the base structures of TET and CIPF were obtained from PubChem and corrected for protonation states and charge using ChemDraw)

further work is required to explore the impact of different chemical activation methods and/or dual chemical activation on the structure and performance of ASBS. Detailed surface and chemical characterization using techniques such as BET and XPS is essential to better understand the structure–activity relationship and adsorption mechanisms. However, this was a limitation in the present work due to the low yield of biochar obtained in each activation cycle. Future work should therefore focus on optimizing the synthesis yield to enable more comprehensive surface and chemical characterization. Moreover, it is important to note that the column experiments in this study were conducted at laboratory scale using an adsorbent bed of 0.025 g to simulate continuous-flow behavior under controlled conditions. This setup provides valuable preliminary insights for the design and optimization of larger-scale applications by generating initial breakthrough data and estimating key design parameters such as adsorption capacity, breakthrough time, and model constants. However, future research should consider pilot-scale or full-scale column studies to validate the practical applicability of ASBS in real-world treatment scenarios.

Further applicability of ASBS for removal of other classes of pharmaceuticals and simultaneous removal of these compounds from wastewater and groundwater should be examined. Moreover, prior to the application of ASBS in wastewater treatment plants, it is crucial to evaluate the potential of the adsorbent in removing lower concentrations of TET and CIPF, as well as to study any potential negative effects of ASBS, which were the focus of our previously published study (Shirani et al., 2024).

Additionally, while the experimental data were reproducible with low standard deviations, future studies should include a larger number of replicates to enable comprehensive variability and confidence assessments. Moreover, the regeneration and reusability of ASBS were not evaluated in the present study due to the preliminary nature of this investigation, which focused on fundamental adsorption performance. However, for determining the practical feasibility and cost-effectiveness of the material assessing its regeneration efficiency over multiple cycles is essential and should be prioritized in future research.

4 Conclusion

The results indicate that *A. sylvestris*-derived activated biochar (ASBS), prepared through a simple and low-cost method using locally available biomass, is an effective adsorbent for removing different classes of pharmaceuticals, including amphoteric and ionic compounds, due to its porous structure and abundant functional groups. This adsorbent demonstrated high and fast adsorption efficiency for ionizable antibiotics, with kinetics best described by the PSO model. The Langmuir model revealed that the maximum adsorption capacities for TET and CIPF removal by ASBS were 402.7 mg g^{-1} and 582.2 mg g^{-1}, respectively. The fixed-bed column study revealed that the breakthrough and exhaustion times were directly influenced by flow rate and the adsorbate concentration, providing valuable data for scaling up continuous treatment systems.

The primary interaction mechanisms involved include electrostatic interactions, π-π EDA interactions, H-bonding and cation-π bonds. Therefore, ASBS is a promising, environmentally friendly adsorbent with potential scalability for practical wastewater treatment applications to remove persistent antibiotic residues before discharge into the environment. Future research should focus on regeneration and reuse studies to assess the long-term performance and economic feasibility of ASBS in continuous operations.

Authors Contributions Conceptualization, Z.Sh.; methodology, Z.Sh.; validation, Z.Sh.; investigation, Z.Sh.; resources, Z.Sh.; data curation, Z.Sh.; writing—original draft preparation, Z.Sh.; writing—review and editing, Z.Sh., V.N., and J.S.; supervision, Z.Sh.; funding acquisition, Z.Sh., and V.N. All authors have read and agreed to the published version of the manuscript.

Funding Open access funding provided by University of Eastern Finland (including Kuopio University Hospital). This research was partially supported by Jenny and Antti Wihuri Foundation for a project on microplastic toxicity awarded to V. Carrasco-Navarro. (Part of the author's time was contributed to this study during the duration of this project.)

Data Availability Data will be made available on request.

Declarations

Ethical Approval Not applicable. This study did not involve any human or animal subjects and therefore did not require ethical approval.

Consent to Participate Not applicable.

Consent for Publication Not applicable.

Competing interest The authors declare that they have no known competing financial interests or personal relationships that could have appeared to influence the work reported in this paper.

References

Acosta, R., Fierro, V., de Yuso, A. M., Nabarlatz, D., & Celzard, A. (2016). Tetracycline adsorption onto activated carbons produced by KOH activation of tyre pyrolysis char. *Chemosphere, 149*, 168–176.

Ajala, O. A., Akinnawo, S. O., Bamisaye, A., Adedipe, D. T., Adesina, M. O., Okon-Akan, O. A., Adebusuyi, T. A., Ojedokun, A. T., Adegoke, K. A., & Bello, O. S. (2023). Adsorptive removal of antibiotic pollutants from wastewater using biomass/biochar-based adsorbents. *RSC Advances, 13*, 4678–4712.

Ali, M. E., El-Aty, A. M. A., Badawy, M. I., & Ali, R. K. (2018). Removal of pharmaceutical pollutants from synthetic wastewater using chemically modified biomass of green alga *Scenedesmus obliquus*. *Ecotoxicology and Environmental Safety, 151*, 144–152.

Ali, S. M., Ashour, B., Farahat, M. G., & El-Sherif, R. M. (2024). Biomass-based perovskite/graphene oxide composite for the removal of organic pollutants from wastewater. *Ceramics International, 50*, 49085–49094.

Álvarez-Torrellas, S., Garrido-Zoido, J. M., López-Maldonado, E. A., Hernández-Abreu, A. B., Águeda, V. I., Delgado, J. A., Gil, M. V., & García, J. (2024). Highlighting the adsorption mechanism of a fluoroquinolone antibiotic from wastewater on carbon xerogel by experiments, characterization, modelling and DFT simulation. *Environmental Science and Pollution Research, 31*, 61795–61818.

Bazkiaee, H. K., Sharifian, S., Asasian-Kolur, N., Najafi, H., Pirbazari, A. E., & Harasek, M. (2024). Efficient removal of tizanidine and tetracycline from water: A single and competitive sorption approach using carboxymethyl cellulose granulated iron-pillared clay. *Applied Surface Science Advances, 21*, 100600.

Bharathi, K. S., & Ramesh, S. P. T. (2013). Fixed-bed column studies on biosorption of crystal violet from aqueous solution by *Citrullus lanatus* rind and *Cyperus rotundus*. *Applied Water Science, 3*, 673–687.

Biswal, B. K., & Balasubramanian, R. (2022). Adsorptive removal of sulfonamides, tetracyclines and quinolones from wastewater and water using carbon-based materials: Recent developments and future directions. *Journal of Cleaner Production, 349*, 131421.

Brinzila, C., Pacheco, M., Ciríaco, L., Ciobanu, R., & Lopes, A. (2012). Electrodegradation of tetracycline on BDD anode. *Chemical Engineering Journal, 209*, 54–61.

Das, S., Dash, S. K., & Parida, K. (2018). Kinetics, isotherm, and thermodynamic study for ultrafast adsorption of azo dye by an efficient sorbent: Ternary Mg/(Al Fe) layered double hydroxides. *ACS Omega, 3*, 2532–2545.

Dhiman, N., & Sharma, N. (2018). Batch adsorption studies on the removal of ciprofloxacin hydrochloride from aqueous solution using ZnO nanoparticles and groundnut (*Arachis hypogaea*) shell powder: A comparison. *Indian Chemical Engineer, 61*(1), 67–78.

Dubinin, M. M., & Radushkevich, L. (1947). Equation of the characteristic curve of activated charcoal. *Chem. Zentr, 1*, 875.

Fiori, I., Santacruz, W., Dionisio, D., & Motheo, A. J. (2022). Electro-oxidation of tetracycline in ethanol-water mixture using DSA-Cl2 anode and stimulating/monitoring the formation of organic radicals. *Chemosphere, 308*, 136487.

Freundlich, H. (1909). *Kolloidchemie*. Akad. Verlagsgeselschaft.

Genç, N. (2015). Removal of antibiotic ciprofloxacin hydrochloride from water by kandira stone: Kinetic models and thermodynamic. *Global Nest Journal, 17*, 498–507.

Gholami, P., Khataee, A., Soltani, R. D. C., Dinpazhoh, L., & Bhatnagar, A. (2020). Photocatalytic degradation of gemifloxacin antibiotic using Zn-Co-LDH@ biochar nanocomposite. *Journal of Hazardous Materials, 382*, 121070.

Guler, U. A., & Sarioglu, M. (2014). Removal of tetracycline from wastewater using pumice stone: Equilibrium, kinetic and thermodynamic studies. *Journal of Environmental Health Science and Engineering, 12*, 79.

Guo, J., Hu, Z., Xie, Z., Yao, Z., Lin, Z., & Huang, W. (2024a). Adsorption of tetracycline by nitrogen-enriched biochar prepared at different pyrolysis temperatures: Considering the crucial role of nitrogen configuration. *Journal of Analytical and Applied Pyrolysis, 179*, 106482.

Guo, Z., Han, X., Zhang, C., He, S., Liu, K., Hu, J., Yang, W., Jian, S., Jiang, S., & Duan, G. (2024b). Activation of biomass-derived porous carbon for supercapacitors: A review. *Chinese Chemical Letters, 35*, 109007.

Halldórsson, G. (2012). ReNo: restoration of damaged ecosystems in the Nordic Countries. Nordic Council of Ministers.

Hamscher, G., Sczesny, S., Höper, H., & Nau, H. (2002). Determination of persistent tetracycline residues in soil fertilized with liquid manure by high-performance liquid chromatography with electrospray ionization tandem mass spectrometry. *Analytical Chemistry, 74*, 1509–1518.

He, J., Dai, J., Zhang, T., Sun, J., Xie, A., Tian, S., Yan, Y., & Huo, P. (2016). Preparation of highly porous carbon from sustainable α-cellulose for superior removal performance of tetracycline and sulfamethazine from water. *RSC Advances, 6*, 28023–28033.

Ho, Y.-S., & McKay, G. (1999). Pseudo-second order model for sorption processes. *Process Biochemistry, 34*, 451–465.

Huang, L., Wang, M., Shi, C., Huang, J., & Zhang, B. (2014). Adsorption of tetracycline and ciprofloxacin on activated carbon prepared from lignin with H_3PO_4 activation. *Desalination and Water Treatment, 52*, 2678–2687.

Inyang, M., & Dickenson, E. (2015). The potential role of biochar in the removal of organic and microbial contaminants from potable and reuse water: A review. *Chemosphere, 134*, 232–240.

Jahangiri-Rad, M., Jamshidi, A., Rafiee, M., & Nabizadeh, R. (2014). Adsorption performance of packed bed column for nitrate removal using PAN-oxime-nano Fe 2 O 3. *Journal of Environmental Health Science and Engineering, 12*, 90.

Jeganathan, Y., Asharp, T., & Nadarajah, K. (2024). Adsorptive behavior of engineered biochar/hydrochar for tetracycline removal from synthetic wastewater. *Environmental Pollution, 345*, 123452.

Ji, L., Wan, Y., Zheng, S., & Zhu, D. (2011). Adsorption of tetracycline and sulfamethoxazole on crop residue-derived ashes: Implication for the relative importance of black carbon to soil sorption. *Environmental Science & Technology, 45*, 5580–5586.

Kumar, A., Bhattacharya, T., Shaikh, W. A., Chakraborty, S., Sarkar, D., & Biswas, J. K. (2022). Biochar modification methods for augmenting sorption of contaminants. *Current Pollution Reports, 8*, 519–555.

Lagergren, S. K. (1898). About the theory of so-called adsorption of soluble substances. *Sven Vetenskapsakad Handingarl, 24*, 1–39.

Langmuir, I. (1918). The adsorption of gases on plane surfaces of glass, mica and platinum. *Journal of the American Chemical Society, 40*, 1361–1403.

Li, H., Zhang, D., Han, X., & Xing, B. (2014). Adsorption of antibiotic ciprofloxacin on carbon nanotubes: PH dependence and thermodynamics. *Chemosphere, 95*, 150–155.

Liao, P., Zhan, Z., Dai, J., Wu, X., Zhang, W., Wang, K., & Yuan, S. (2013). Adsorption of tetracycline and chloramphenicol in aqueous solutions by bamboo charcoal: A batch and fixed-bed column study. *Chemical Engineering Journal, 228*, 496–505.

Liu, P., Liu, W.-J., Jiang, H., Chen, J.-J., Li, W.-W., & Yu, H.-Q. (2012). Modification of bio-char derived from fast pyrolysis of biomass and its application in removal of tetracycline from aqueous solution. *Bioresource Technology, 121*, 235–240.

Liu, H., Xu, G., & Li, G. (2021). Preparation of porous biochar based on pharmaceutical sludge activated by NaOH and its application in the adsorption of tetracycline. *Journal of Colloid and Interface Science, 587*, 271–278.

Liu, S., Huang, J., Zhang, W., Shi, L., Yi, K., Zhang, C., Pang, H., Li, J., & Li, S. (2022). Investigation of the adsorption behavior of Pb (II) onto natural-aged microplastics as affected by salt ions. *Journal of Hazardous Materials, 431*, 128643.

Lopez-Ramon, M. V., Stoeckli, F., Moreno-Castilla, C., & Carrasco-Marin, F. (1999). On the characterization of acidic and basic surface sites on carbons by various techniques. *Carbon, 37*, 1215–1221.

Lu, Y., Wang, H., Lu, Y.-Y., Ren, Z.-Q., Gao, N., Wang, J.-J., Huang, B.-C., & Jin, R.-C. (2025). In-situ synthesis of lanthanum-coated sludge biochar for advanced phosphorus adsorption. *Journal of Environmental Management, 373*, 123607.

Ma, J., Yang, M., Yu, F., & Zheng, J. (2015). Water-enhanced removal of ciprofloxacin from water by porous graphene hydrogel. *Scientific Reports, 5*, 13578.

Magnússon, S.H. (2011). NOBANIS-invasive alien species fact sheet-anthriscus sylvestris. Database Eur. Netw. Invasive Alien Species.

Mangla, D., Sharma, A., & Ikram, S. (2022). Critical review on adsorptive removal of antibiotics: Present situation, challenges and future perspective. *Journal of Hazardous Materials, 425*, 127946.

Mao, H., Wang, S., Lin, J.-Y., Wang, Z., & Ren, J. (2016). Modification of a magnetic carbon composite for ciprofloxacin adsorption. *Journal of Environmental Sciences, 49*, 179–188.

Martins, A. C., Pezoti, O., Cazetta, A. L., Bedin, K. C., Yamazaki, D. A., Bandoch, G. F., Asefa, T., Visentainer, J. V., & Almeida, V. C. (2015). Removal of tetracycline by NaOH-activated carbon produced from macadamia nut shells: Kinetic and equilibrium studies. *Chemical Engineering Journal, 260*, 291–299.

Miller, T. W., & D'auria, D. E. (2011). Effects of herbicide, tillage, and grass seeding on wild chervil (*Anthriscus sylvestris*). *Invasive Plant Science and Management, 4*, 326–331.

Mohamed Nasser, S., Abbas, M., & Trari, M. (2024). Understanding the rate-limiting step adsorption kinetics onto biomaterials for mechanism adsorption control. *Progress in Reaction Kinetics and Mechanism, 49*, 14686783241226858.

Nasir, M., Shahid, D., Khan, W., Afroz, A., Samdani, M.S., Rashid, M.A.R.M.A. (2025). Mechanistic insights into paracetamol adsorption from water using ZnO nanoparticle-immobilized chitosan-inulin composites: fractal kinetics, statistical physics, thermodynamic analysis, and application to real water samples. *Environmental Science: Water Research & Technology*

Nazari, G., Abolghasemi, H., Esmaieli, M., & Pouya, E. S. (2016). Aqueous phase adsorption of cephalexin by walnut shell-based activated carbon: A fixed-bed column study. *Applied Surface Science, 375*, 144–153.

Oruganti, R. K., Pal, D., Panda, T. K., Shee, D., & Bhattacharyya, D. (2023). Green synthesis of calcium oxide nanoparticles impregnated activated carbon from algal–bacterial activated sludge: Its application in ciprofloxacin removal. *International Journal of Environmental Science and Technology, 20*, 12379–12396.

Panwar, N. L., & Pawar, A. (2022). Influence of activation conditions on the physicochemical properties of activated biochar: A review. *Biomass Conversion and Biorefinery, 12*, 925–947.

Peiris, C., Gunatilake, S. R., Mlsna, T. E., Mohan, D., & Vithanage, M. (2017). Biochar based removal of antibiotic sulfonamides and tetracyclines in aquatic environments: A critical review. *Bioresource Technology, 246*, 150–159.

Peñafiel, M. E., Matesanz, J. M., Vanegas, E., Bermejo, D., Mosteo, R., & Ormad, M. P. (2021). Comparative adsorption of ciprofloxacin on sugarcane bagasse from Ecuador and on commercial powdered activated carbon. *Science of the Total Environment, 750*, 141498.

Peng, X., Hu, F., Lam, F. L., Wang, Y., Liu, Z., & Dai, H. (2015). Adsorption behavior and mechanisms of ciprofloxacin from aqueous solution by ordered mesoporous carbon and bamboo-based carbon. *Journal of Colloid and Interface Science, 460*, 349–360.

Pérez-Morales, J. M., Sánchez-Galván, G., & Olguín, E. J. (2019). Continuous dye adsorption and desorption on an invasive macrophyte (*Salvinia minima*). *Environmental Science and Pollution Research, 26*, 5955–5970.

Pezoti, O., Cazetta, A. L., Bedin, K. C., Souza, L. S., Martins, A. C., Silva, T. L., Júnior, O. O. S., Visentainer, J. V., & Almeida, V. C. (2016). NaOH-activated carbon of high surface area produced from guava seeds as a high-efficiency adsorbent for amoxicillin removal: Kinetic, isotherm and thermodynamic studies. *Chemical Engineering Journal, 288*, 778–788.

Rivera-Utrilla, J., Gómez-Pacheco, C. V., Sánchez-Polo, M., López-Peñalver, J. J., & Ocampo-Pérez, R. (2013). Tetracycline removal from water by adsorption/bioadsorption on activated carbons and sludge-derived adsorbents. *Journal of Environmental Management, 131*, 16–24.

Sayğılı, H., & Güzel, F. (2016). Effective removal of tetracycline from aqueous solution using activated carbon prepared from tomato (*Lycopersicon esculentum* Mill.) industrial processing waste. *Ecotoxicology and Environmental Safety, 131*, 22–29.

Seegers, C. L., Tepper, P. G., Setroikromo, R., & Quax, W. J. (2018). Cytotoxic deoxypodophyllotoxin can be extracted in high purity from *Anthriscus sylvestris* roots by supercritical carbon dioxide. *Planta Medica, 84*, 544–550.

Selmi, T., Sanchez-Sanchez, A., Gadonneix, P., Jagiello, J., Seffen, M., Sammouda, H., Celzard, A., & Fierro, V. (2018). Tetracycline removal with activated carbons produced by hydrothermal carbonisation of *Agave americana* fibres and mimosa tannin. *Industrial Crops and Products, 115*, 146–157.

Sharma, S., Umdor, R. S., Longchar, I. T., Ezung, S. L., & Sinha, D. (2024). Exploring the adsorption of catechol and resorcinol onto *Croton caudatus* activated carbon: An integrated experimental and theoretical approach. *Groundwater for Sustainable Development, 27*, 101325.

Shirani, Z., Santhosh, C., Iqbal, J., & Bhatnagar, A. (2018). Waste *Moringa oleifera* seed pods as green sorbent for efficient removal of toxic aquatic pollutants. *Journal of Environmental Management, 227*, 95–106.

Shirani, Z., Song, H., & Bhatnagar, A. (2020). Efficient removal of diclofenac and cephalexin from aqueous solution using *Anthriscus sylvestris*-derived activated biochar. *Science of the Total Environment, 745*, 140789.

Shirani, Z., Carrasco-Navarro, V., Majlesi, S., Yli-Pirilä, P., Kukkonen, J. V., & Akkanen, J. (2024). Efficiency and ecotoxicity of activated biochar in the treatment of artificial wastewater contaminated by pharmaceuticals. *Journal of Environmental Management, 371*, 123224.

Singh, A., Pratap, S. G., & Raj, A. (2024). Occurrence and dissemination of antibiotics and antibiotic resistance in aquatic environment and its ecological implications: A review. *Environmental Science and Pollution Research, 31*, 47505–47529.

Sips, R. (1948). On the structure of a catalyst surface. *Journal of Chemical Physics, 16*, 490–495.

Sun, B., Li, D., Linghu, W., & Guan, X. (2018). Degradation of ciprofloxacin by manganese (III) intermediate: Insight into the potential application of permanganate/bisulfite process. *Chemical Engineering Journal, 339*, 144–152.

Swenson, H., & Stadie, N. P. (2019). Langmuir's theory of adsorption: A centennial review. *Langmuir, 35*, 5409–5426.

Taheran, M., Naghdi, M., Brar, S. K., Knystautas, E. J., Verma, M., Ramirez, A. A., Surampalli, R. Y., & Valéro, J. R. (2016). Adsorption study of environmentally relevant concentrations of chlortetracycline on pinewood biochar. *Science of the Total Environment, 571*, 772–777.

Tan, X., Liu, Y., Zeng, G., Wang, X., Hu, X., Gu, Y., & Yang, Z. (2015). Application of biochar for the removal of pollutants from aqueous solutions. *Chemosphere, 125*, 70–85.

Tan, X., Liu, S., Liu, Y., Gu, Y., Zeng, G., Cai, X., Yan, Z., Yang, C., Hu, X., & Chen, B. (2016). One-pot synthesis of carbon supported calcined-Mg/Al layered double hydroxides for antibiotic removal by slow pyrolysis of biomass waste. *Scientific Reports, 6*, 39691.

Tong, Y., McNamara, P. J., & Mayer, B. K. (2019). Adsorption of organic micropollutants onto biochar: A review of relevant kinetics, mechanisms and equilibrium. *Environmental Science. Water Research & Technology, 5*, 821–838.

Vieno, N., Hallgren, P., Wallberg, P., Pyhälä, M., Zandaryaa, S., Baltic Marine Environment Protection Commission, (2017). Pharmaceuticals in the aquatic environment of the Baltic Sea region: a status report. UNESCO Publishing.

Vyas, A., Shukla, S., Pandey, R., Jain, V., Joshi, V., & Gidwani, B. (2012). Chervil: A multifunctional miraculous nutritional herb. *Asian Journal of Plant Sciences, 11*, 163.

Wang, L., Ying, G.-G., Zhao, J.-L., Yang, X.-B., Chen, F., Tao, R., Liu, S., & Zhou, L.-J. (2010). Occurrence and risk assessment of acidic pharmaceuticals in the Yellow River, Hai River and Liao River of north China. *Science of the Total Environment, 408*, 3139–3147.

Wang, H., Fang, C., Wang, Q., Chu, Y., Song, Y., Chen, Y., & Xue, X. (2018). Sorption of tetracycline on biochar derived from rice straw and swine manure. *RSC Advances, 8*, 16260–16268.

Wang, Y., Xu, L., Wei, F., Ding, T., Zhang, M., & Zhu, R. (2022). Insights into the adsorption mechanism of tetracycline on hierarchically porous carbon and the effect of nanoporous geometry. *Chemical Engineering Journal, 437*, 135454.

Wilson, M. P., & Worrall, F. (2021). The heat recovery potential of 'wastewater': A national analysis of sewage effluent

discharge temperatures. *Environmental Science. Water Research & Technology, 7*, 1760–1777.

Xu, Y., Fan, Z., Li, X., Yang, S., Wang, J., Zheng, A., & Shu, R. (2024). Cooperative production of monophenolic chemicals and carbon adsorption materials from cascade pyrolysis of acid hydrolysis lignin. *Bioresource Technology, 399*, 130557.

Yu, F., Sun, S., Han, S., Zheng, J., & Ma, J. (2016). Adsorption removal of ciprofloxacin by multi-walled carbon nanotubes with different oxygen contents from aqueous solutions. *Chemical Engineering Journal, 285*, 588–595.

Yu, Z., Chen, H., Zhang, J., Sun, W., Li, T., Qiu, Z., & Younas, M. (2025). Ultra-high selective removal of Congo red and Ciprofloxacin using unusual LDO modified biochar: Influence of emerging pollutants and application attempts. *Separation and Purification Technology, 352*, 128108.

Zeng, Z., Tan, X., Liu, Y., Tian, S., Zeng, G., Jiang, L., Liu, S., Li, J., Liu, N., & Yin, Z. (2018). Comprehensive adsorption studies of doxycycline and ciprofloxacin antibiotics by biochars prepared at different temperatures. *Frontiers in Chemistry, 6*, 80.

Zeng, Z., Ye, S., Wu, H., Xiao, R., Zeng, G., Liang, J., Zhang, C., Yu, J., Fang, Y., & Song, B. (2019). Research on the sustainable efficacy of g-MoS2 decorated biochar nanocomposites for removing tetracycline hydrochloride from antibiotic-polluted aqueous solution. *Science of the Total Environment, 648*, 206–217.

Zhang, Y., Zhu, C., Liu, F., Yuan, Y., Wu, H., & Li, A. (2019). Effects of ionic strength on removal of toxic pollutants from aqueous media with multifarious adsorbents: A review. *Science of the Total Environment, 646*, 265–279.